

Accepted Manuscript

Rationally designed hecogenin thiosemicarbazone analogs as novel MEK inhibitors for the control of breast malignancies

Heba E. Elsayed, Hassan Y. Ebrahim, Eman G. Haggag, Amel M. Kamal, Khalid A. El Sayed

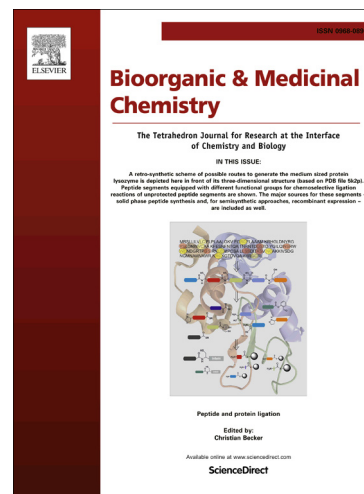
PII: S0968-0896(17)31493-1
DOI: <https://doi.org/10.1016/j.bmc.2017.09.033>
Reference: BMC 13993

To appear in: *Bioorganic & Medicinal Chemistry*

Received Date: 20 July 2017
Revised Date: 16 September 2017
Accepted Date: 21 September 2017

Please cite this article as: Elsayed, H.E., Ebrahim, H.Y., Haggag, E.G., Kamal, A.M., El Sayed, K.A., Rationally designed hecogenin thiosemicarbazone analogs as novel MEK inhibitors for the control of breast malignancies, *Bioorganic & Medicinal Chemistry* (2017), doi: <https://doi.org/10.1016/j.bmc.2017.09.033>

This is a PDF file of an unedited manuscript that has been accepted for publication. As a service to our customers we are providing this early version of the manuscript. The manuscript will undergo copyediting, typesetting, and review of the resulting proof before it is published in its final form. Please note that during the production process errors may be discovered which could affect the content, and all legal disclaimers that apply to the journal pertain.



Article

Rationally designed hecogenin thiosemicarbazone analogs as novel MEK inhibitors for the control of breast malignancies

Heba E. Elsayed^{a,b}, Hassan Y. Ebrahim^a, Eman G. Haggag^b, Amel M. Kamal^b, Khalid A. El Sayed^{a*}

^aDepartment of Basic Pharmaceutical Sciences, School of Pharmacy, University of Louisiana at Monroe, Monroe, Louisiana, USA, 71201.

^bDepartment of Pharmacognosy, Faculty of Pharmacy, Helwan University, Helwan, Cairo, Egypt, 11795.

*Correspondence: Professor Khalid El Sayed, Department of Basic Pharmaceutical Sciences, School of Pharmacy, University of Louisiana at Monroe, 1800 Bienville Drive, Monroe, Louisiana 71201, USA. Phone: +1-318-342-1725; Fax: +1-318-342-1737; E-mail: elsayed@ulm.edu

Abstract

Natural products have documented oncology success history as valuable scaffolds for selective target modulation. Herein, the sapogenin hecogenin (**1**) was screened for its anti-breast cancer inhibitory capacity using *in vitro* assays, including proliferation, cytotoxicity, migration, invasion assays, and western blotting. The results identified **1** as a propitious hit with modest activities attributed to the concurrent down regulation of mitogen activated protein kinase kinase/extracellular signal-regulated kinase (MEK) distinctive downstream effectors. Guided by *in silico* 3D-structural insights of MAPK kinase domain, an extension-strategy was adopted at **1**'s C-3 and C-12 aimed at the design of novel hecogenin-based analogs with improved target binding affinity. Thirty-three analogs were prepared and tested, among which hecogenin 12-(3'-methylphenyl thiosemicarbazone) (**30**) displayed the most potent selective anticancer effects. Analog **30** demonstrated antiproliferative, antimigratory and anti-invasive activities at low μM level, compared to the negligible effect on the non-tumorigenic MCF-10A mammary epithelial cells. Durable regression of breast tumor xenografts in athymic nude mice was observed after treatments with **30**, compared to its parent hecogenin at the same dose regimen, confirmed the hit-to-lead promotion of this analog. Hecogenin-12-thiosemicarbazones, represented by **30**, is a novel MEK inhibitory lead class to control breast neoplasms.

Keywords: Antiproliferative, Breast cancer, Hecogenin, MEK inhibitor, Rational design, Thiosemicarbazones.

1. Introduction

Steroidal sapogenins encompass a structurally diverse class of natural products that possess non-polar, 27-carboncore skeleton.¹ They have received considerable attention as potential precursors for semisynthesis of various pharmaceutically valuable derivatives, as cortisone and other related corticosteroids.¹ Spirostanes represent a distinct class of steroidal sapogenins with a spiroketal side chain.² Hecogenin (**1**) is a ubiquitous spirostane abundant in plants of the genus *Agave* (sisal, Agavaceae) and perhaps the only known naturally occurring 12-oxo-spirostane steroidal sapogenin. Manifold biological activities have been reported for **1**, particularly anticancer.²⁻⁵ Sapogenin **1** has been subjected to various chemical transformations aimed at optimizing its anti-neoplastic activity. Examples of **1**'s prior semisynthetic manipulation are the cleavage or modifications of the spirostane side-chain to cholestanic analogs with selective antitumor activity.^{6,7} Moreover, many aliphatic esters of hecogenin have been semisynthesized and exploited in this regard; particularly hecogenin acetate. Hecogenin acetate was identified as a suitable and economical starting material for multiple complex anticancer entities. Fortunately, it is incorporated in the convergent synthesis of the cephalostatins, ritterazines and hippuristanol.^{8,9} Reportedly, hecogenin acetate modulated various key cell signaling events as extracellular signal-regulated kinases (ERK1/2) phosphorylation and matrix metalloproteinase-2 (MMP-2) production as well as interference with reactive oxygen species (ROS) production.¹⁰

Thiosemicarbazones deemed an outstanding pharmacophoric core, with self-complementary hydrogen bonding motif in diverse antiprotozoal, antiviral, antibacterial and antitumor entities.¹¹⁻¹⁴ The antitumor activity of thiosemicarbazone-containing structures perhaps is due to the moon-lightening mechanisms, such as inhibiting ribonucleotide reductase (RR),

ROS production, inhibiting topoisomerase II and more recently inhibiting multidrug resistance protein 1 (MDR1).¹⁵⁻¹⁷ The immense significance of thiosemicarbazones as potential pharmacophoric moiety in drug design is documented.

Cancer is among the main health concerns worldwide and one of the primary medicinal chemistry and pharmacology targets.¹⁸ Breast cancer is the most common malignancy affecting females worldwide.¹⁸ Moreover, breast cancer is considered the leading cause of disability-adjusted life-years globally attributed to lack of effective early diagnosis and selective treatment options.¹⁹ Chemotherapy is still the established forefront treatment alternative for many cancer patients, however selectivity and off-target side effects are major concerns.¹⁹ Intent transition from cytotoxic chemotherapy to molecularly-targeted cancer therapy resulted in astonishing successful therapies, with significant safety and improved response rates.²⁰ Blockade of protein phosphorylation is amongst the clinically validated auspicious targets in cancer control. Protein phosphorylation is a decisive reversible post-translational mechanism, which is controlled through various protein kinases that are capable to phosphorylate on tyrosine (Tyr), serine (Ser), or threonine (Thr). Dual-specificity kinases are those that overall belong to Ser/Thr kinase group.²¹ Protein kinase inhibitors are molecules aimed at protein phosphorylation inhibition and interrogate specific intracellular signaling. Imatinib, an inhibitor of the oncogenic kinase BCR-Abelson murine leukemia viral oncogene homolog 1 (AbI1) in chronic myelogenous leukemia, was the first protein kinase-targeting anticancer drug followed by several other examples.²²

Rat sarcoma small GTPase/rapidly accelerated fibrosarcoma kinase/mitogen activated protein kinase kinase/extracellular signal-regulated kinase (RAS/RAF/MEK/ERK) is an organized conserved eukaryotic signaling pathway.²³ The signaling module is the driver behind paramount cellular processes such as gene transcription, cellular proliferation, and survival.^{24,25}

The Ser/Thr kinases MEK1/2 specifically phosphorylate and activate ERK1/2.^{26,27} The activated ERK is dimerized thereafter, regulating various targets in the cytosol and translocate to the nucleus where it phosphorylates a variety of transcription factors regulating gene expression. The clinical trial out comes of selumetinib (AZD6244), a potent selective MEK1 inhibitor, was reported in 2008 and showed significant improvements in patients with advanced cancers.²⁸ On the other hand, in case of patients with advanced melanoma harboring N-RAS/B-RAF mutations, binimetinib (MEK162) was endorsed as a contemporary MEK1/2 inhibitor.²⁹ Recently, FDA approved the first pan-MEK1/2 inhibitor, trametinib (Mekinist™), for the treatment of metastatic melanoma.³⁰ However, despite the considerable progress on new molecularly targeted therapies, discovery of more potent, targeted MEK lead inhibitors is still a dire therapeutic need.

This study reports the rational design of semisynthetic hecogenin analogs with improved *in vitro* anti-breast cancer activities through targeting MEK kinase domain. Rational design targeted C-3 and C-12 ester, semicarbazone and thiosemicarbazone hybrid extensions to improve MEK kinase domain binding affinity, anti-breast cancer activity and selectivity. The thiosemicarbazone **30** reigned supreme in *in vitro* and *in vivo* anticancer potencies and had no toxic effects on the non-tumorigenic mammary epithelial MCF-10A cell growth. Western blot analysis revealed that **30**'s anticancer effect is, at least in part, mediated by the blockade of MEK activation with subsequent inhibition of the downstream mitogenic signaling. **30** markedly reduced tumor growth in orthotopic breast cancer xenograft model compared to its parent **1** without overt toxicity signs. Collectively, the present findings suggest the hecogenin-12-thiosemicarbazones, represented by **30**, as a promising MEK inhibitory lead entity with a potential to control breast malignancies associated with aberrant MEK activity.

2. Results and discussion

Hecogenin (**1**), a ubiquitous spirostanoic steroidal sapogenin in sisal wastes, has been previously described for its anticancer activity.³ Therefore, **1** was screened *in vitro* for ability to inhibit breast cancer proliferation, migration, and invasion. The antiproliferative effect of **1** was assessed against a panel of six human mammary carcinoma cell lines endowed by diverse molecular and phenotypic characteristics. For instance, estrogen receptor (ER α) is expressed in the luminal A-type MCF-7 and T-47D cell lines; while SKBR-3 and the luminal B-type BT-474 are human epidermal growth factor receptor 2 (HER2) overexpressing ones. On the other hand, the claudin low MDA-MB-231 and the basal MDA-MB-468 were negative for the triple receptors; ER α , HER2 and progesterone receptor (PR) and so alternatively named, triple negative breast cancer (TNBC) cell lines.³¹ Sapogenin **1** exhibited modest antiproliferative activity with IC₅₀ values in the mid μ M level (Figure 1). Thus, it was reasonable to hypothesize that **1** target a common pathway(s) involved in the proliferation and survival of breast cancer cells.

Hecogenin-3-*O*-acetate's ability to modulate the extracellular signal-regulated kinases (ERK1/2) phosphorylation was previously reported and evidenced by Western blot analysis.¹⁰ ERK is the only downstream substrate for the non-receptor hydrophilic protein mitogen-activated protein kinase/extracellular signal-regulated kinase (MEK). MEK1/2 phosphorylate, activate and spark ERK1/2-mediated oncogenic proliferation and differentiation pathways.^{26,27} A computational docking experiment was accomplished using Glide 5.8 module³² in standard mode to explore the virtual binding modes of **1** and hence explore potential future rational design of more potent semisynthetic analogs. Careful inspection of the prepared dual-specific MEK protein kinase revealed its resemblance to alternative protein kinases in having a multifunctional, small N-terminal lobe, protein kinase cleft and large C-terminal lobe comprising several conserved α -

helices and β -strands.³³ Sapogenin **1** was anchored within the generated grid constraints of MEK cavity with a notable docking score of -7.9.

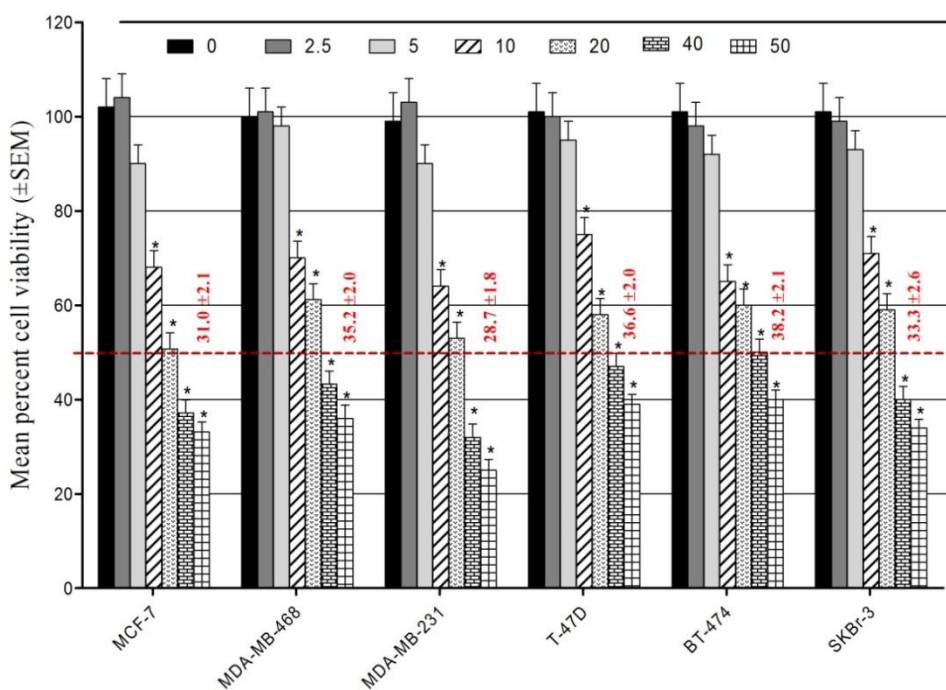


Figure 1. Effect of sapogenin **1** treatments on the proliferation of multiple human breast cancer cell lines. Displayed is the mean percent cell viability at different concentrations of **1** after 72 h incubation. The red dashed line showed the calculated IC₅₀ ± SEM for each cell line.

The space-filling model assumed **1** in an extended spatial conformation, consistent with the general horizontal dimensions of the pocket, leaving behind the C-3 hydroxyl and C-12 ketone enough spaces to accommodate structure extensions (Figure 2). Interestingly, **1** displayed favorable H-bond bridge by the C-3 OH group with the gatekeeper Met146 carbonyl backbone allocated in the hinge region, while the rear pyran oxygen displayed a H-bond interaction with Lys192 terminal amino in the catalytic loop. Accordingly, **1** was hypothesized as a potential MEK inhibitory scaffold amenable for semisynthetic optimizations at C-3 hydroxyl and C-12 ketone owing to the vacant room prevailed behind.

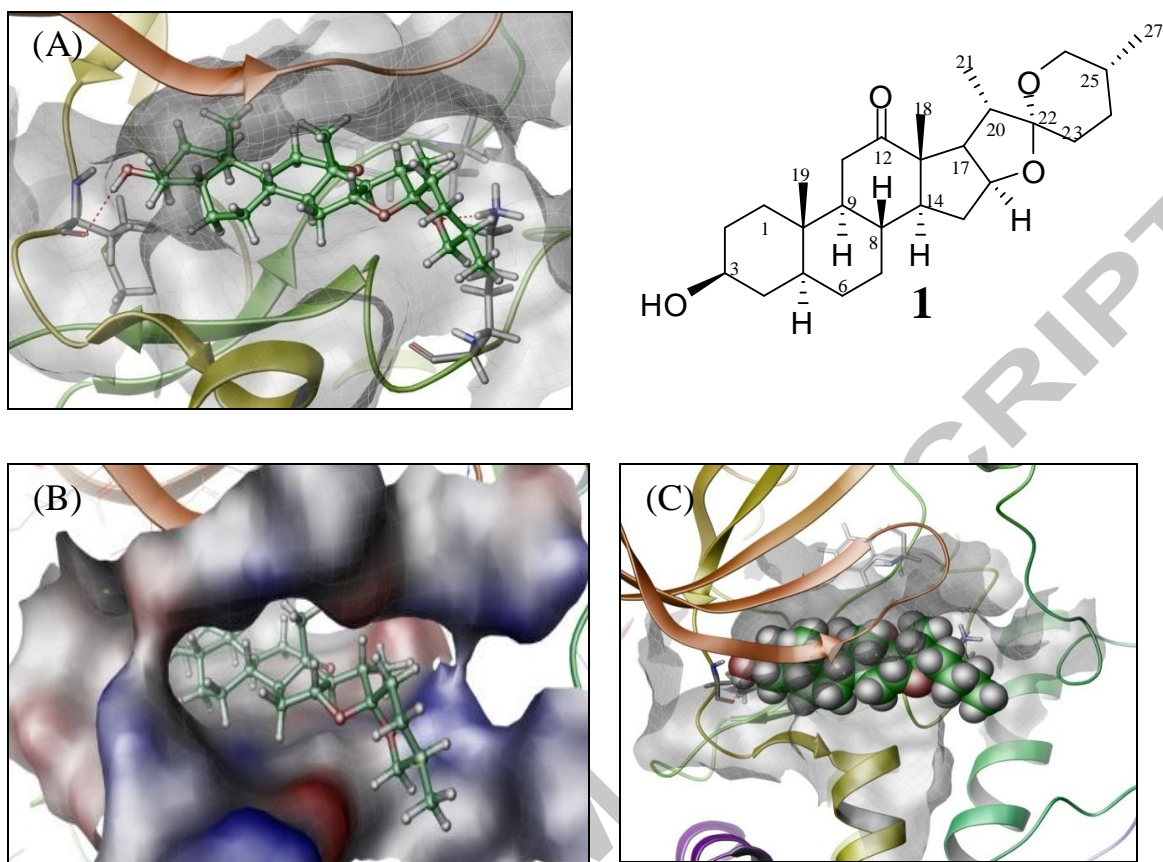
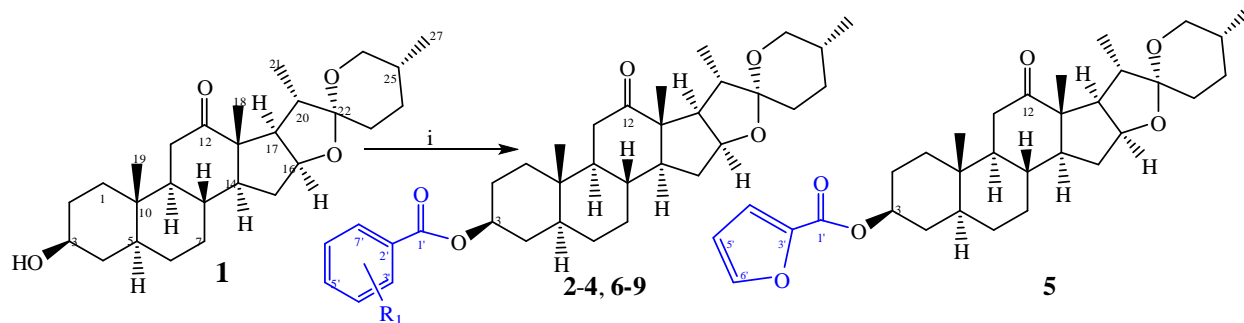


Figure 2. Overview of the binding of **1** in green (ball and stick cartoon or CPK format) with MEK kinase domain (PDB: 3EQF) represented as a ribbon diagram. The protein is oriented as for the canonical kinase domain, with the N-terminal lobe at the top and the C-terminal lobe at the bottom. The three figures are from a similar vantage point, displayed in space-filling model the good fitting of **1** within the identified grid. **1** Displayed favorable H-bond interactions with residues Met146 and Lys192, while enough space around C-3 hydroxyl and C-12 ketone likely to accommodate subsequent structure extensions.

The first optimization direction of **1** aimed at C-3 spacer domain via esterification of C-3 secondary alcohol. This was implemented through base-catalyzed esterification reaction of **1** with various aromatic acid chlorides (Scheme 1), affording the corresponding ester analogs **2-9**.

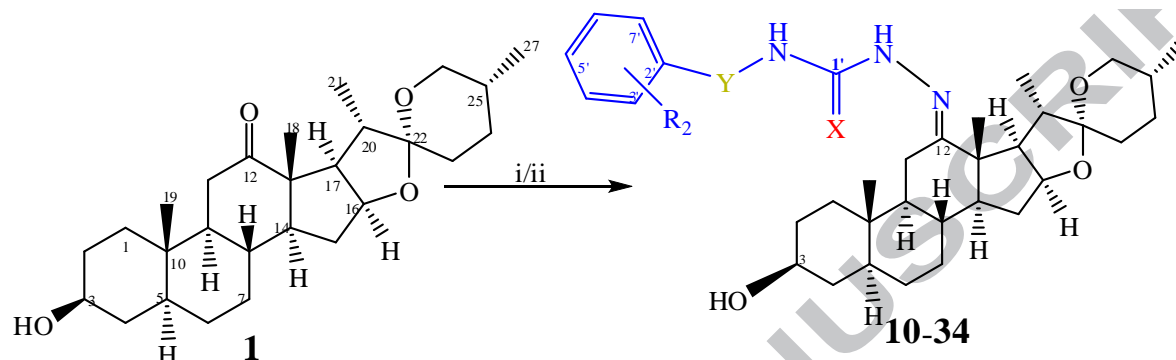


Scheme 1. General semisynthetic route to hecogenin ester analogs **2-9**. Reagents and conditions: (i) Acid chloride, pyridine, DMAP, RT, overnight.

Purified products were fully characterized by 1D and 2D NMR spectroscopy and mass spectrometry. For instance, 3-*O*-hecogenin benzoyl ester (**2**) displayed a downfield shift of H-3 to δ 4.90 (+1.3 ppm), along with its corresponding carbon C-3 by +4.0 ppm (δ 75.0), compared to the parent **1**, confirming the C-3 esterification.

The human triple negative breast cancer (TNBC) MDA-MB-231 cells are best known for their mutant RAS and RAF proteins and showed high levels of phosphorylated ERK (p-ERK) expression, indicating active MAPK pathway.³⁴ Additionally, MDA-MB-231 cells were optimally sensitive to **1**'s treatments in MTT proliferation assay (Figure 1). Thus, semisynthesized esters were evaluated for their antiproliferative potency on the surveyed panel of breast adenocarcinoma cell lines, while their SAR was configured according to their activity against MDA-MB-231 cells. Results demonstrated that ester analogs showed inconsiderable improvement in **1**'s antiproliferative activity (Table 1). This may be attributed, at least in-part, to potential hydrophobic interactions with the proximity amino acids that replaced the free C-3 OH interactions, which may stipulate the significance of the C-3 OH group to anchorage at the target kinase's hinge region. Subsequent optimizations maintained free C-3 OH group and targeted C-12 spacer in **1** to probe additional binding interactions. An extension strategy was adopted using a hydrophilic linker capable to interplay H-bond bridges with the target, meanwhile come to an

end with lipophilic functionalized substituent directed towards the target hydrophobic cleft. Hence, a cross-coupling reaction using various commercially available phenyl semicarbazides and phenyl thiosemicarbazides appropriately functionalized on the aromatic ring was successfully achieved (Scheme 2).



Scheme 2. Semisynthesis of hecogenin phenylsemicarbazone **10-14** and hecogenin thiosemicarbazones **15-34**. Reagents and conditions: (i) Semicarbazide.HCl, EtOH, Pyridine, RT, 6 h. (ii) Semicarbazide/thiosemicarbazide, EtOH, RT, overnight.

The aimed products were purified, isolated in moderate to excellent yields and elucidated using 1D and 2D NMR spectroscopy and mass spectrometry. Careful inspection of the ^{13}C -PENDANT NMR spectrum of hecogenin-12-(phenyl semicarbazone) (**10**) and hecogenin-12-(phenyl thiosemicarbazone) (**15**) revealed the replacement of **1**'s C-12 ketone signal (δ_{C} 213.4) with new ones at δ_{C} 158.5 or 159.9, corresponding to their new C-12 imine carbonyls, respectively. The new imine carbonyl carbons showed 3J HMBC cross interactions with the C-18 methyl proton singlets (δ_{H} 0.98-1.00). Moreover, the integrity of urea or thiourea fragment was based on their C-1' carbonyl or thiocarbonyl at δ_{C} 154.6 or δ_{C} 176.3, respectively. Meanwhile, the broad singlet signals at δ 8.50-9.50 were ascribable to the two aza-methines of the urea fragment, manifesting 2J HMBC correlations with the C-1' carbonyl and thiocarbonyl or the C-2' quaternary aromatic carbons. In addition, one of the aza-methines showed a 3J HMBC correlation with the C-12 imine carbonyl. While *E* and *Z*-geometrical isomers are possible for the

non-symmetric semicarbazone and thiosemicarbazone products, it is interesting to note that evidence for such isomeric mixtures was not observed by 1D NMR experiments, suggested the presence of only one isomer. The ^1H - ^1H NOESY spectrum indicated the exclusive oxime double bond *E*-geometry orientation in **30**, based on the cross peak interactions between the hydrazine NH singlet (δ 8.70) and H₂-11 methylene proton at δ 1.92. This assignment was in agreement with the literature, which the preference to the less sterically hindered *E*-isomer product of such reactions.³⁵ Thus, the same double bond geometry was also assumed in rest of analogs.

Analog **10-34** were evaluated for their antiproliferative activities against the TNBC MDA-MB-231 cell line. In fact, the improved activity of hecogenin-12-phenylsemicarbazone (**10**), compared to the parent **1** ($\text{IC}_{50} = 9.2\ \mu\text{M}$) encouraged additional optimizations. Various analogs with substituted phenyl ring that featured different steric, hydrophobic, and electronic properties were synthesized and tested merely to perceive better activity. For instance, the electron withdrawing hybrids represented by analogs **11-13**; *m*-chlorophenyl, *p*-chlorophenyl and *m*-trifluoromethyl phenyl semicarbazones, respectively, (**13**) were semisynthesized and tested. The chlorinated analogs declared ahead improvement in potency compared to **10** (Table 1), even though the positional effect of the Cl atom seems to have a significant role in the activity. The *para*-positioned chlorinated analog declared better potency than its *meta*-congener (Table 1). On the other hand, unexpectedly the *meta*-substituted analog **13**, bearing trifluoromethyl phenyl moiety showed a significant activity decrease ($\text{IC}_{50} = 14.0\ \mu\text{M}$), drawing the attention to the position-activity discriminatory effects. Interestingly, while examining the urea linker optimal span, the tosyl semicarbazone analog **14** revealed significantly reduced activity compared to **10** (Table 1), suggesting the four-atom hydrazine carbothioamide hydrophilic linker is optimal for possible for target affinity and subsequent cellular activity. This was also supported by the

literature use of "soft" donor atoms, as sulfur in thiosemicarbazone scaffolds for good anticancer activity.³⁶ Hecogenin-12-phenyl thiosemicarbazone (**15**) exhibited the expected improved potency ($IC_{50} = 7.8 \mu M$), compared to its phenyl semicarbazone counterpart **10**, proving the activity preference for thiosemicarbazones. The impact of electronic effects of different chloro, fluoro, nitro, and trifluoromethyl phenyl-substituted thiosemicarbazones **16-25** was then studied. The 3'-trifluoromethyl-bearing analog **23** exhibited the most attained potency of this group ($IC_{50} = 2.1 \mu M$). On the other hand, the electron-donating functionalities were also explored through synthesizing and biological testing of methoxy (**26-27**), phenoxy (**28**), ethyl (**29**), methyl (**30-33**) and methylenedioxy (**34**) phenyl thiosemicarbazone analogs. Notably, the 3'-methyl analog **30** exhibited the utmost potency against a panel of breast cancer cell lines (Table 1 and Figure 3), spotlighting the final requirement of an optimal mono-substituted, hydrophobic, sterically tolerable phenyl substituent. Hence, analog **30** was selected for a comprehensive activity study.

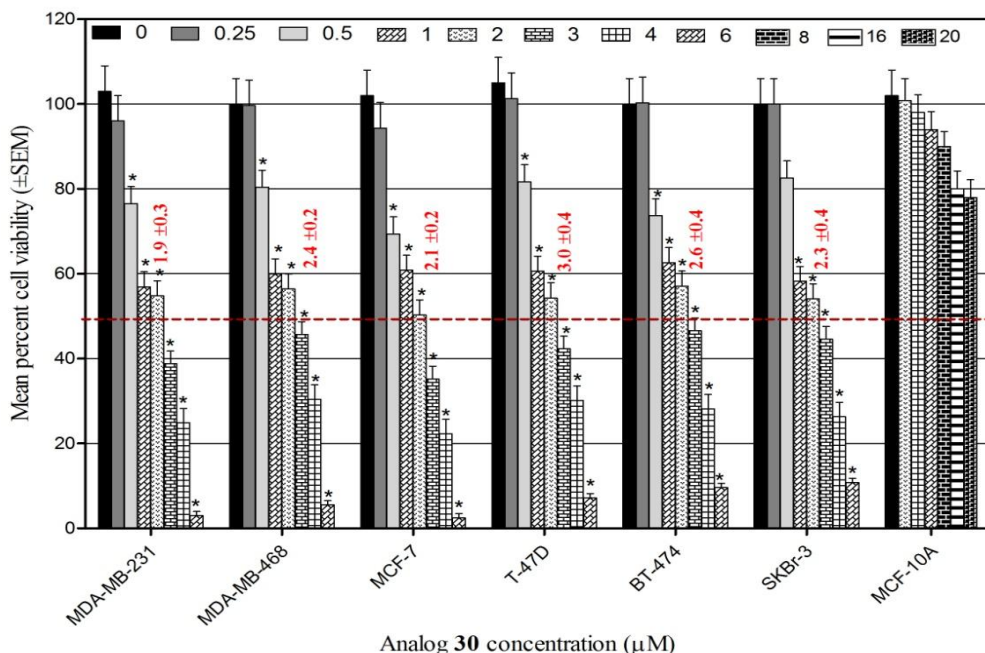


Figure 3. Effect of analog **30** treatments on multiple human breast cancer cell lines and the human non-tumorigenic mammary epithelial cells MCF-10A. Displayed is the mean percent cell

viability at different concentrations of **30** after treatment incubation period. The red dashed line showed calculated $IC_{50} \pm SEM$ of **30** for each cell line.

Molecular docking of **30** within the prepared MEK kinase domain showed that it is quite closely overlaps with its parent **1**, with better extension towards the hydrophobic pocket, affording an excellent docking score of -9.0. The imine nitrogen displayed a H-bond bridge with the amino acid Ser194, meanwhile the *E*-configuration enabled the substituted phenyl thio-semicarbazone fragment to be well-fitted within a hydrophobic pocket clustered with Val127, Ile141, Cys207, Leu74 and Met143 residues, generating an excellent hydrophobic interaction. Interestingly, the distal phenyl moiety in **30** displayed parallel-displaced stacking with Phe209 allocated within the Asp-Phe-Gly (DFG) motif, while the *ortho*-methyl functionality predominantly contributed a hydrophobic interaction with Cys207-methylene. The thiourea linker formed a H-bond interaction with the Lys97's positively charged terminal amino group (Figure 4).

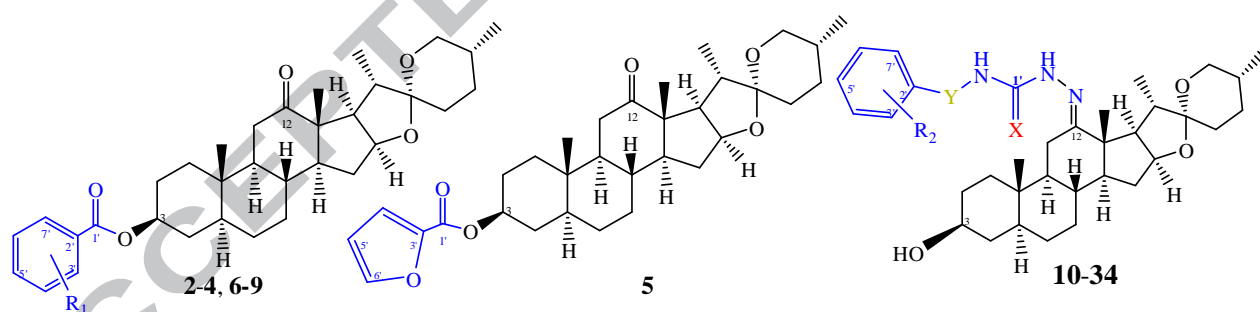


Table 1. *In vitro* antiproliferative activity (IC_{50} (μM) $\pm SE$) of compounds **2-34** against a panel of human breast cancer cell lines.

Cpd No.	R ₁ R ₂		X Y		IC_{50} ($\mu M \pm SEM$)					
	MDA-MB-231	468	MCF-7	BT-474	SKBr3	T-47D				
1	-	-	-	-	28.7 \pm 1.8	35.2 \pm 2.0	31.0 \pm 2.1	38.2 \pm 2.1	33.3 \pm 2.6	36.6 \pm 2.0

2	H	-	-	-	29.1±2.0	34.2±2.2	30.3±2.3	36.3±1.9	33.4±2.0	37.8±3.1
3	4'-Cl	-	-	-	>40.0	>40.0	>40.0	>40.0	>40.0	>40.0
4	3'-OCH ₃	-	-	-	>40.0	>40.0	>40.0	>40.0	>40.0	>40.0
5	-	-	-	-	>40.0	>40.0	>40.0	>40.0	>40.0	>40.0
6	4'-CF ₃	-	-	-	>40.0	>40.0	>40.0	>40.0	>40.0	>40.0
7	5'-F	-	-	-	27.0±1.3	33.4±1.8	28.0±1.4	30.0±1.9	36.0±2.0	29.0±1.9
8	5'-CN	-	-	-	25.7±1.4	32.6±1.9	33.2±1.8	35.0±1.7	34.7±2.3	>40.0
9	5'-NO ₂	-	-	-	25.3±1.7	>40.0	32.4±1.2	>40.0	34.9±1.9	>40.0
10	-	H	O	-	9.2±1.1	11.9±0.9	10.4±0.7	11.9±0.4	12.0±0.7	13.5±0.6
11	-	4'-Cl	O	-	10.0±1.3	10.9±0.7	9.7±0.9	12.0±0.9	9.8±0.8	13.0±0.9
12	-	5'-Cl	O	-	8.5±0.9	11.3±0.8	9.1±1.0	9.8±0.7	9.0±0.9	12.0±0.7
13	-	4'-CF ₃	O	-	14.0±1.2	15.3±1.0	13.8±1.1	19.2±1.5	15.7±0.9	20.9±1.0
14	-	5'-CH ₃	O	SO ₂	28.0±1.5	36.4±1.8	29.3±2.0	>40.0	31.0±1.9	>40.0
15	-	H	S	-	7.8±0.7	8.4±0.7	8.0±0.5	9.3±0.6	9.1±0.8	10.3±1.4
16	-	3'-Cl	S	-	5.5±0.9	6.2±0.5	5.9±0.8	6.5±0.6	5.7±0.7	7.0±0.6
17	-	5'-Cl	S	-	11.5±0.8	12.8±1.2	12.0±0.9	11.8±0.9	14.8±1.2	15.1±1.1
18	-	3',5'-di-Cl	S	-	7.5±0.7	8.0±0.8	7.9±0.6	9.0±0.9	8.8±0.7	9.5±1.0
19	-	3',7'-di-Cl	S	-	6.0±0.9	7.3±0.8	6.4±0.8	6.9±0.7	9.0±0.8	10.4±1.1
20	-	5'-F	S	-	5.0±0.8	4.2±0.7	4.0±0.6	6.3±0.8	4.5±0.7	5.9±0.5
21	-	3'-NO ₂	S	-	4.3±0.8	6.1±0.9	5.0±0.7	6.9±0.9	5.5±0.6	9.0±1.3
22	-	5'-NO ₂	S	-	7.3±0.9	8.0±1.0	7.5±0.9	10.3±1.0	7.9±0.9	11.5±1.2
23	-	3'-CF ₃	S	-	2.1±0.4	2.7±0.5	2.2±0.3	3.1±0.6	2.1±0.3	2.4±0.4
24	-	5'-CF ₃	S	-	3.2±0.5	3.9±0.2	3.7±0.2	4.4±0.6	4.0±0.5	3.8±0.2
25	-	4',6'-di-CF ₃	S	-	7.3±0.8	8.2±0.7	8.0±0.5	10.8±1.0	8.6±0.9	11.0±1.3
26	-	3'-OCH ₃	S	-	6.8±0.7	7.5±0.9	7.1±0.4	8.8±0.6	7.5±0.8	10.2±1.0
27	-	5'-OCH ₃	S	-	9.5±0.9	11.2±2.0	10.1±1.4	10.9±0.9	11.5±1.3	14.2±0.8
28	-	5'-O-ph	S	-	28.1±1.7	30.8±2.0	27.0±1.6	31.2±1.8	29.0±2.1	>40
29	-	3'-CH ₂ CH ₃	S	-	3.8±0.8	5.8±0.4	5.0±0.7	8.3±0.7	4.7±0.4	8.8±1.1
30	-	3'-CH ₃	S	-	1.9±0.3	2.4±0.2	2.1±0.2	2.6±0.4	2.3±0.4	3.0±0.4
31	-	5'-CH ₃	S	-	3.1±0.7	4.0±0.8	3.7±0.9	4.5±0.9	3.8±0.5	6.1±0.8
32	-	3',5'-di-CH ₃	S	-	2.7±0.4	3.8±0.4	3.0±0.6	3.7±0.7	4.2±0.3	5.2±0.4
33	-	3',7'-di-CH ₃	S	-	2.3±0.3	2.8±0.5	2.5±0.2	3.2±0.4	2.9±0.5	4.2±0.7
34	-	3',5'- (-O-CH ₂ -O-)	S	-	5.5±0.8	5.9±0.9	5.3±0.4	7.5±0.9	6.2±0.8	7.8±0.9

Green highlight: parent (hecogenin); **Violet highlights:** parent of each optimization group; **Pink highlight:** the most active semisynthetic analog.

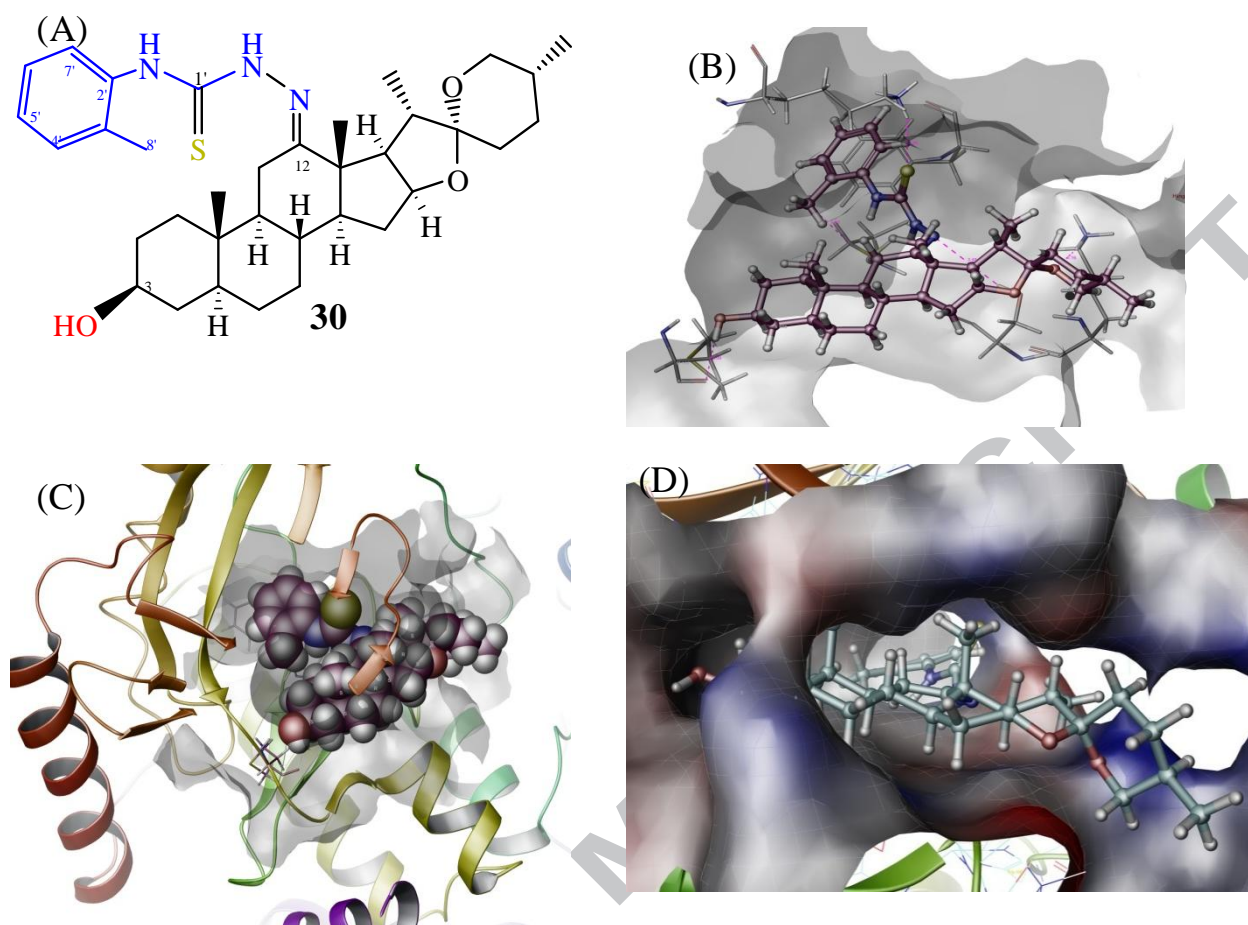


Figure 4. Binding mode of analog **30** at the MEK kinase domain (PDB: 3EQF). A. Chemical structure of **30**. B. Ribbon diagram of the binding pose of **30** (maroon ball and stick cartoon) at the MEK kinase domain. This space-filling model revealed the good fitting of **30** within the proximity of Phe209 and Cys207 residues satisfying the C-12 extension tactic. C. Binding pose of **30** within the MEK kinase domain using CPK format. D. Space filling model showing the protein target canonical kinase domain, with the N-terminal lobe at the top and the C-terminal lobe at the bottom. All parts are from a similar vantage point.

To add further justification to the docking results, the native ligand of the MEK crystal structure (PDB: 3EQF) was docked into its ATP binding site, applying the same parameters which have been used for docking analog **30** (Figure 5). The bound conformation of co-crystallized ligand was obtained with a good root mean square displacement (RMSD) of 0.2 Å, suggesting the robustness of the docking experiments. In the investigated MEK crystal structure PDB 3EQF, **30** demonstrated partial overlay with almost the same interactions (Figure 5).

Together, *in silico* data suggested the potential of **30** as a propitious MEK inhibitory hit appropriate for further validation.

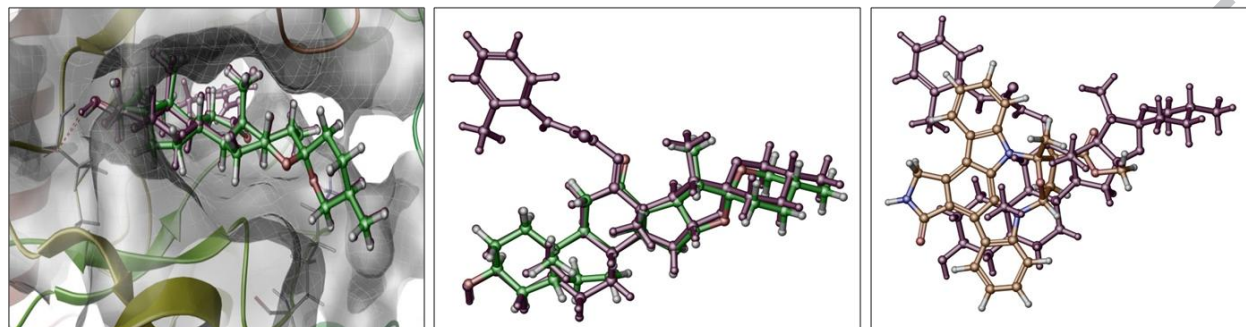


Figure 5. (a) Overview of MEK domain (PDB: 3EQF) represented as a ribbon diagram in complex with **1** in green and **30** in maroon with ball and stick cartoon format. (B) Superposition of **1** in green and **30** in maroon with ball and stick cartoon format. (C) Superposition of K252A (MEK ATP-competitive inhibitor in orange) with **30** in maroon.

Many therapies, while killing the bulk of cancerous cells, may ultimately fail to discriminate normal healthy cells from their purported malignant cells. Accordingly, anticancer selectivity of **30** was evaluated using the human mammary epithelial cell line MCF-10A. These cells are immortalized and non-tumorigenic with some features of normal breast epithelium, including lack of anchorage-independent growth and dependence on growth factors and hormones for proliferation and survival.³⁷ Cells were exposed to various concentrations of **30** as stated per experimental section. The results showed that **30**'s various treatments (1-20 μM) displayed non-significant effect on MCF-10A viability, compared to their respective vehicle control-treated group, reinforcing the **30**'s selective anticancer effect towards malignant breast cells.

Measurement of intracellular contents leakage through impaired plasma membrane has been widely used to assess chemical cytotoxicity.³⁸ Lactate dehydrogenase (LDH) is a soluble cytoplasmic enzyme allocated in almost all cells and is released into extracellular space in

respond to plasma membrane destruction.³⁸ Therefore; the detection of LDH in the culture medium can be used as a marker for cytotoxicity. Herein, the Cayman's LDH cytotoxicity assay kit was used to evaluate the ability of **30** to induce the LDH release in MDA-MB-231 cells in comparison to its parent **1**. Four different doses of tested compounds were used to assess targeted cell death. Sapogenin **1** showed 27.8 % cytotoxicity at the maximum tested dose (100 μ M), which is more than three-fold its reported antiproliferative IC₅₀. Analog **30** achieved 5.9% cytotoxicity at the maximum tested dose (10 μ M), which is more than five-fold its reported antiproliferative IC₅₀ (Table 2). This clearly suggested that **30** did not show significant cytotoxicity up to several-fold its antiproliferative IC₅₀ values and therefore its effect is mainly due cytostatic, which is among distinctive features for targeted therapies.

Table 2. Percent cytotoxicity of **1** and **30** evaluated by LDH release from MDA-MB-231 cells.

	Triton X Hecogenin (1)					Analog 30			
Conc. (μ M)	10%	25	50	75	100	1.25	2.5	5.0	10.0
%Cytotoxicity	100%	0.04%	2.72%	10.3%	27.8%	0.74%	1.27%	1.80%	5.94%

Although cancer cell proliferation is often regarded as the most important aspect of cancer progression, however, other key aspects play a crucial role in cancer progression and metastasis, including migration and invasion.³⁹ Hence, interfering with both processes could have positive impacts on patient survival. The inhibitory effects of **1** on the migration and invasion capacities of the highly metastatic MDA-MB-231 cells using wound-healing (WHA) and CultreCoat[®] invasion assays, respectively, was probed at various non-toxic doses. In WHA, after the confluent cancerous cells exposed to a treatment period of 24 h, **1** significantly repressed the MDA-MB-231 cells migration towards the denuded zone in a direct function of increasing efficacy with treatment concentrations (Figure 6B). Treatment with **30** resulted in a dose-dependent cell migration inhibition, with a calculated IC₅₀ of 2.5 μ M (Figure 6B).

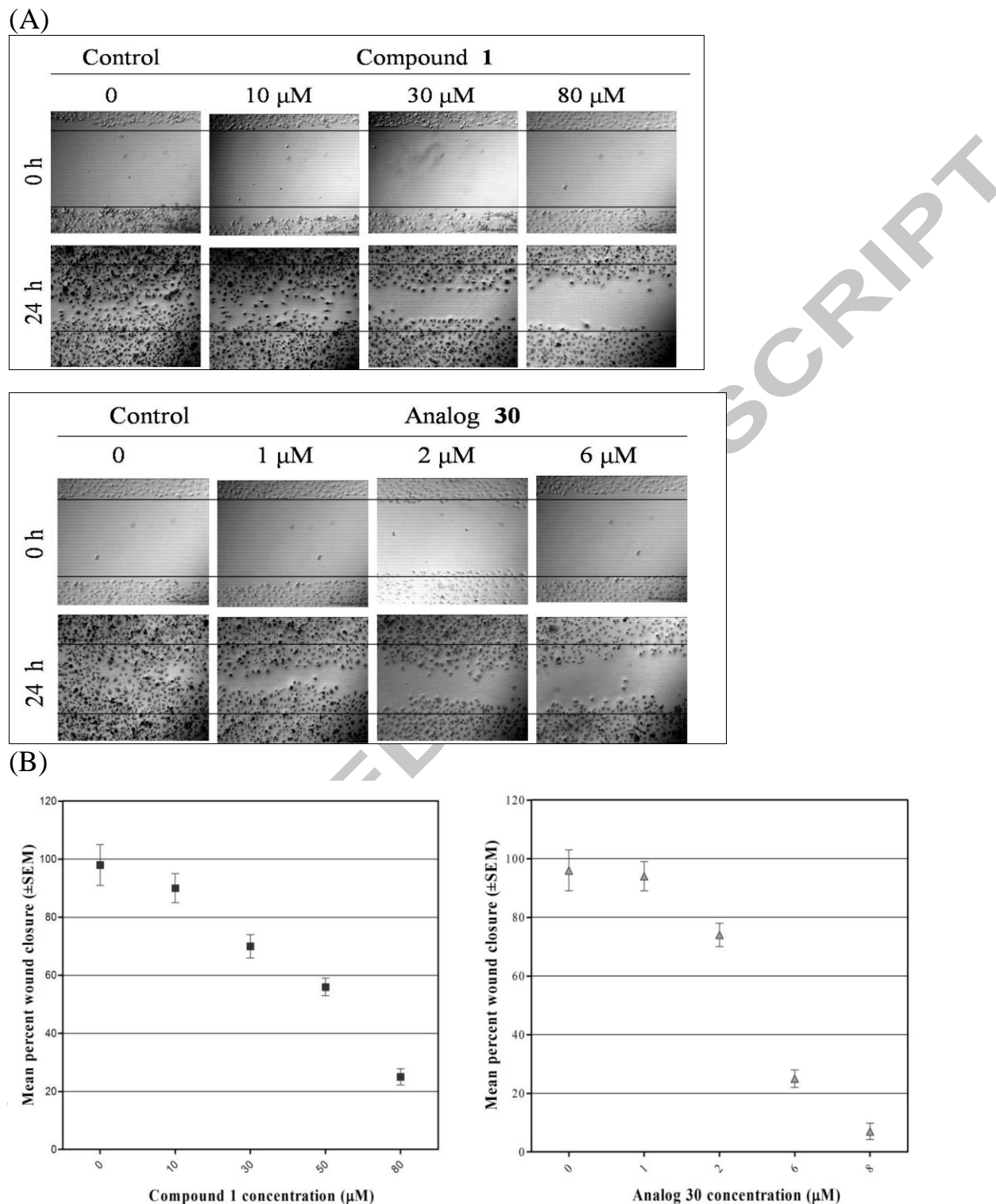
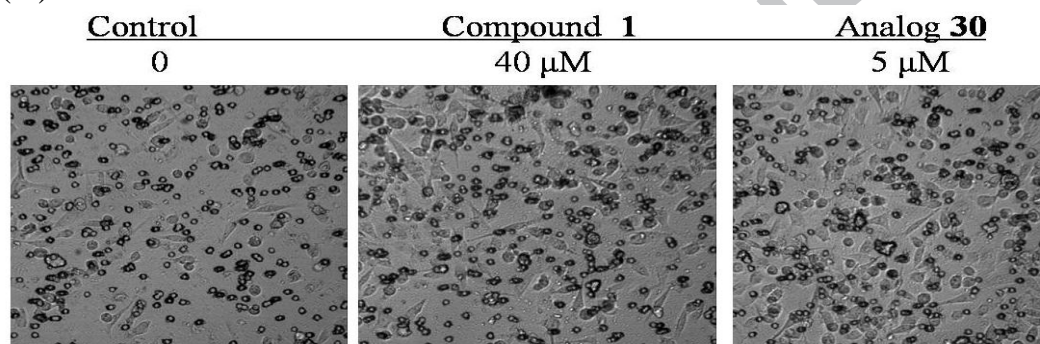


Figure 6. Effects of **1** and **30** on the TNBC MDA-MB-231 cells migration capacity using WHA. (A) Representative microscopic images of created wounds at zero time and 24 h post-incubation with vehicle as negative control or various treatment concentrations. (B) Dose response curve of **1** and **30** treatments versus percent wound closure.

On the other hand, **1** and **30** effects on MDA-MB-231 cells invasion across the extracellular matrix was probed at four different doses. 24 h post plating, most of seeded cells within the control group invaded the coating extract, thus the upper surface comprised minimal cell density. Analog **30** significantly inhibited cancerous cells invasion, with maximum percent invasion inhibition calculated as 92.4% at 5 μ M (maximum tested dose) indicated by higher cell density at the upper surface of the invasion chamber (Fig. 7). On the other hand, treatment with **1** at the maximum tested dose (80 μ M) significantly inhibited cell invasion, with 86.2% invasion inhibition (Fig. 7). The calculated IC₅₀ for **30** was 2.2 μ M, compared to 37.1 μ M for the parent **1**.

(A)



(B)

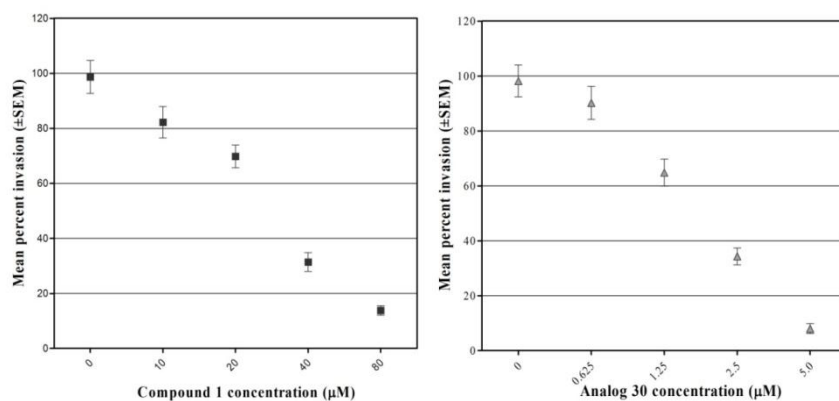


Figure 7. Effects of analog **30**, compared to its parent **1** against the TNBC MDA-MB-231 cells invasive capacity using CultreCoat[®] cell invasion assay. (A) Representative microscopic images of upper chambers (non-invasive cell density) with the vehicle, **1** or **30**. (B) Dose response effect of **1** and **30** treatments versus average percent cell invasion.

Invasive breast cancer subtypes, including TNBC MDA-MB-231 cells, are associated with augmented aberrant cellular proliferation and invasiveness pathways, just as the mitogen-

activated protein kinases (MAPKs).³⁴ MAPK regulates diverse cellular programs that coordinately regulate cell proliferation, differentiation, motility, and survival. The wide range of functions regulated by the MAPK is mediated through phosphorylation of several downstream substrates, including members of a family of protein kinases termed MAPK-activated protein kinases (MAPKAPKs) as mitogen- and stress-activated kinases (MSKs) and MAPK-interacting kinases (MNKs).^{40,41}

Accordingly, to confirm the MEK inhibitory activity of **30**, Western blot analyses was implemented using MDA-MB-231 cells lysate, following administration of two different doses of each of **1** and **30**, along with a vehicle control treatment. The phosphorylation levels of the specific MEK downstream effector, ERK (MAPK) was significantly reduced in both **1** and **30** treatment groups, compared to vehicle control treatment (Figure 8B). Interestingly, MSK activation was attenuated due to ERK-phosphorylation inhibition, which subsequently, at least in-part, hampered the proliferation, survival, motility and invasiveness of breast cancer cells. Collectively, immunoblot results strongly support the ability of **30** to inhibit MEK catalytic activity and thus interfering with MAPK cellular-related functions.

Significant *in vitro* activity of analog **30** against MDA-MB-231 cells (Table 1) motivated subsequent *in vivo* study is to assess its anticancer efficacy concurrently with its parent **1** in a pertinent breast cancer xenograft model. Athymic nude Foxn1^{nu}/Foxn1⁺ mice orthotopically-transplanted with MDA-MB-231/GFP cells were used. Five days after latency period after tumor cells implantation, solid tumors became palpable. Mice then were intraperitoneally administrated equivalent 10 mg/kg/3X week doses **1** (group I) or **30** (group II), while control group received vehicle only. Treatments were continued for twenty-eight days. Mice were observed and body weights were monitored per dosing for afterwards preliminary toxicity signs. Both treatments

were enduring without overt signs of neither toxicity nor significant body weight change, compared to the vehicle-control group. Consistent with the *in vitro* lack of toxicity against the non-tumorigenic MCF10A mammary epithelial cells, nude mice showed good tolerance to the both treatments. Tumor growth was monitored and quantified. On the basis of caliper measurements, treatment groups manifested significant tumors growth attenuation by the end of the study, compared to the vehicle control group. Hecogenin (**1**) induced 57.4% tumor growth inhibition while analog **30** treatments induced 78.1% tumor inhibition (Table 3 and Figure 9). Ultimately, **30** significantly suppressed cell proliferation and attenuate tumor growth in this orthotopic model of TNBC and therefore qualified as a lead compound.

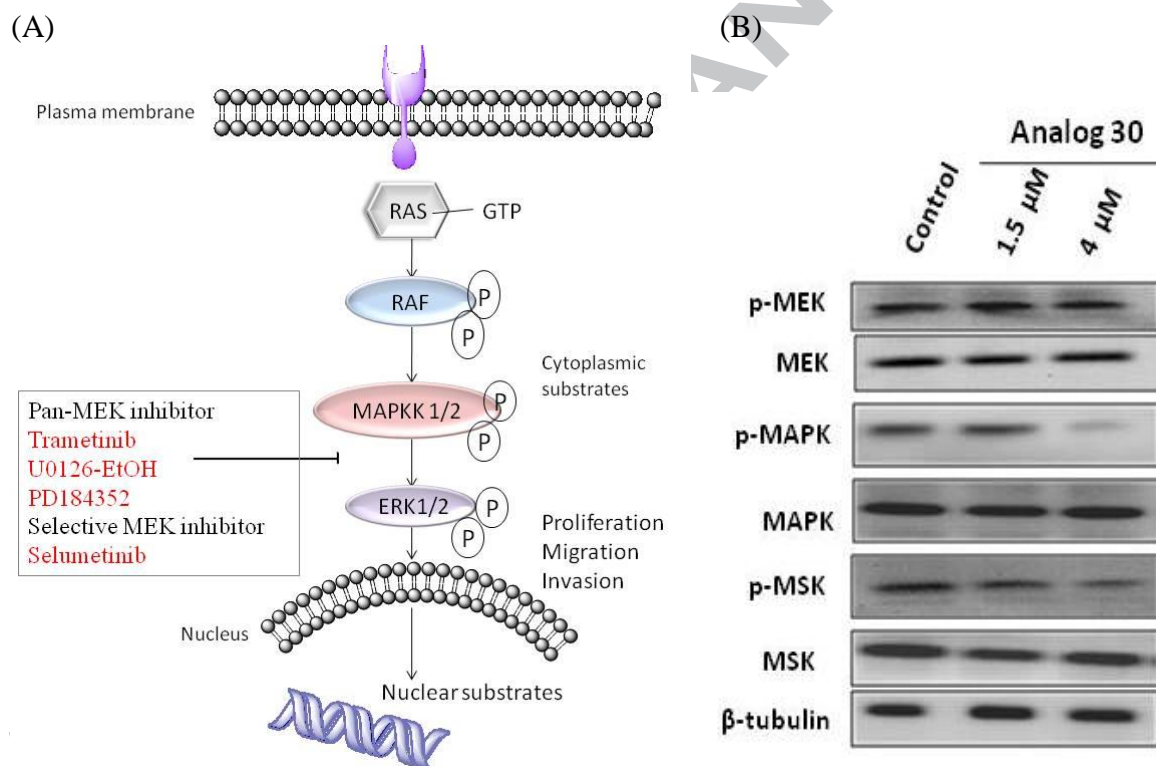


Figure 8. (A) Overview of the MAPK pathway. (B) Western blot analyses of *in vitro* vehicle control and **30** treatments in the TNBC MDA-MB-231 cells. Data show downregulation of activated MAPK kinase and downstream effectors, ERK and MSK in both treatment groups compared to vehicle control.

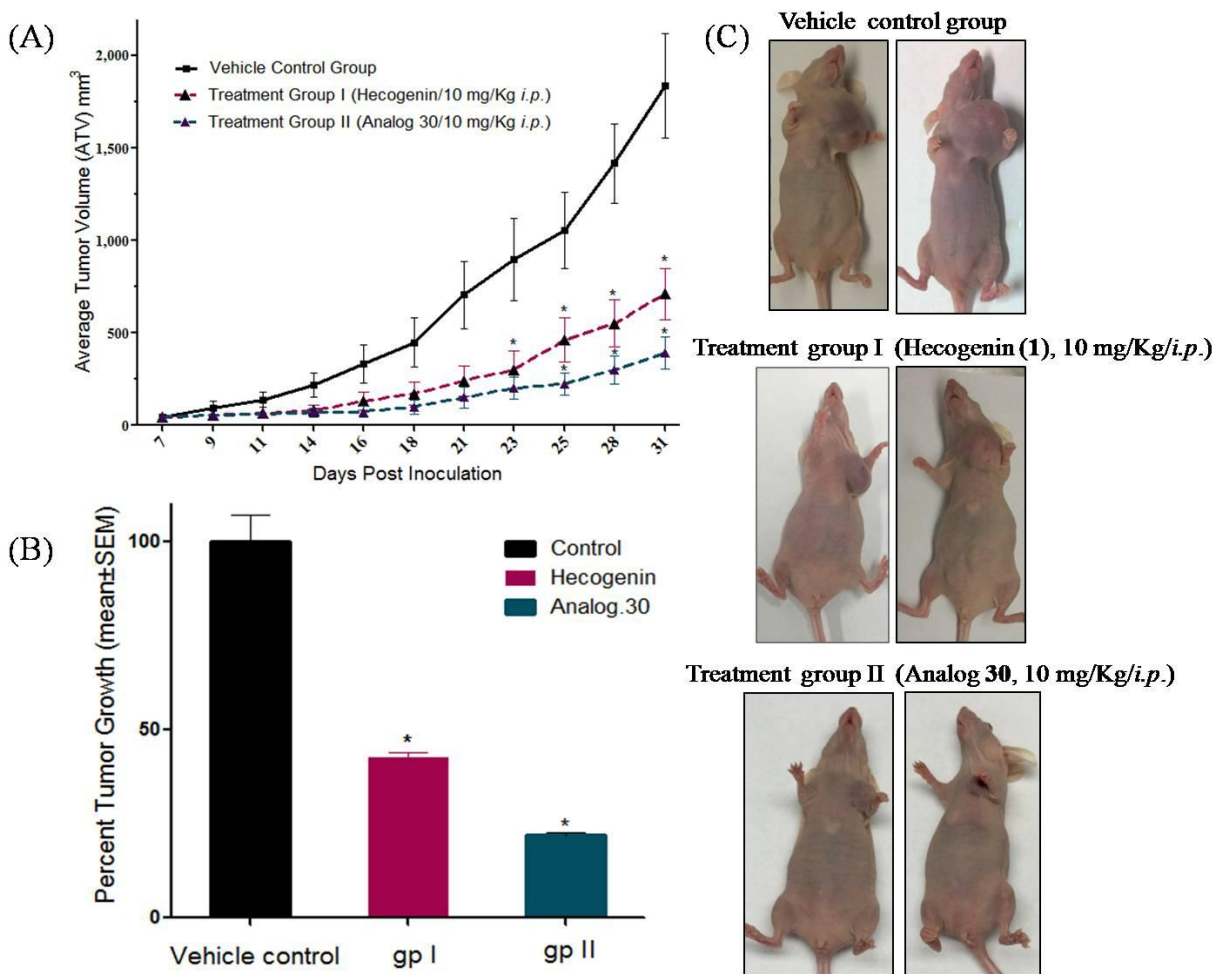


Figure 9. *In vivo* anticancer activities of **1** and **30** against MDA-MB-231/GFP breast cancer cells in athymic nude mouse xenograft model. (A) Effects of **1** and **30** treatments on the mean tumor volume throughout the study compared to vehicle control group. (B) Percent tumor growth (TG) in treatment groups, compared to vehicle control group calculated at the study end. (C) Pictorial representation of mice from control and treatment groups at the study end.

Table 3. *In vivo* anticancer activity of **1** and **30** against the TNBC MDA-MB-231 cells in nude mouse xenograft model.

Group	Initial tumor volume (TV_0)	Final tumor volume (TV_0)	Dose (mg/kg/day)	% Growth inhibition
Control	51.3 \pm 1.9	1837.0 \pm 281.8	-	-
Group I	49.4 \pm 2.7	810.7 \pm 140.2	10 mg	57.36%
Group II	50.2 \pm 1.4	441.3 \pm 88.8	10 mg	78.09%

Conclusions

Rational design of natural products-based semisynthetic analogs is a versatile strategy to optimize parent bioactive hits, improve their lead-like and druggability characters, and promote

them as future clinical candidates. This study identified the natural sapogenin hecogenin (**1**) and its rationally modified semisynthetic analogs as potential MAPK pathway inhibitors for the control of breast malignancies. The thiosemicarbazone analog **30** showed a robust antitumor efficacy that was correlated with the inhibition of MAPK kinase signaling in highly proliferating malignant cells and attenuate their growth and invasiveness. The *in vivo* data reinforced the *in vitro* cellular conclusions and promoted **30** to the lead rank, validating its potential for future use to control breast malignancies with dysregulated MAPK pathway.

Experimental section

General experimental procedures

Thin-layer chromatography analysis was carried on aluminum pre-coated Si gel 60 F₂₅₄ TLC plates (EMD Chemicals Inc., Gibbstown, NJ, USA), while Si gel 60 (230-400 mesh, Natland International Corporation, Morrisville, NC, USA) was used for column chromatography. UV light and freshly prepared *p*-anisaldehyde–methanol–acetic acid–sulfuric acid (2:170:20:10 v/v/v/v) used as a spray reagent for chemical visualization. ¹H and ¹³C NMR spectra were obtained on a JEOL Eclipse ECS-400 NMR spectrometer (Boston, MA, USA) operated at 400 and 100 MHz, respectively. Delta™ NMR Data Processing Software (JEOL Inc., MA, USA) was used for analysis and spectral processing with chemical shifts (δ) reported in parts per million (ppm) relative to internal residual solvent signals (7.26 and 77.1 ppm for CDCl₃; 2.04 and 29.8, 206.3 ppm for acetone-d₆ in ¹H and ¹³C NMR spectra, respectively). NMR data assignments (Tables SI 1-15) were based on PENDANT, ¹H-¹H COSY, ¹H-¹³C HMQC or HMBC experiments. The following abbreviations were used to assign proton signal multiplicities: s (singlet), d (doublet), t (triplet), m (multiplet), dd (doublet of doublet). The ESI-MS carried out on AB Sciex-3200 QTRAP LC/MS/MS system (Applied Biosystems, Foster

City, CA) using Analyst version 1.4.1 software (MDS Sciex; Toronto, Canada). Analytes were ionized using electrospray ionization (ESI) interfaced with standard turbo V ion source.

Chemicals, reagents, and antibodies

All chemicals were purchased from Sigma-Aldrich (St. Louis, MO), unless otherwise stated. The steroidal sapogenin, hecogenin, (purity >90%; Catalog# 230015; CAS # 467-55-0) was purchased from Natland International Incorporation (NC, USA). All reactions were conducted in a well-ventilated fume hood using Teflon-coated magnetic stirrer bars at room temperature. All solvents and reagents were purchased from Sigma-Aldrich (or Alfa Aesar and used without further purification. All yields reported are isolated yields. All antibodies were purchased from Cell Signaling Technologies (Beverly, MA) and used at a dilution of 1:1000.

Chemical synthesis

General procedure for preparation of 3-*O*-hecogenin esters

Hecogenin (40 mg, 0.093 mmol), Et₃N (80 μ L, 0.79 mmol) and DMAP (98 mg, 0.79 mmol) were dissolved in 3 mL dry pyridine. The mixture was stirred at room temperature for 20 min followed by gradual addition of 1.5 equivalents of different acid chlorides. The reaction was set under continuous stirring overnight. Thereafter, water (10 mL) was added to quench the reaction followed by shaking with saturated solution of NaHCO₃ (10 mL x 3). Finally, the aqueous phase was extracted with EtOAc (3 x 5 mL) and the organic layers were pooled, concentrated, and dried over anhydrous Na₂SO₄. The crude mixture was purified using normal phase Si gel 60 column chromatography eluted with *n*-hexanes-acetone 8:2 in isocratic mode to afford analogs **2-9**.

3 β -O-(Benzoyl)-5 α ,25R-spirostan-12-one (**2**)

Following the abovementioned esterification procedure using benzoyl chloride afforded **2** in a 60% yield as a white amorphous powder. TLC: *n*-hexane-acetone, 7:3; ESI-MS *m/z*: 535.3 [M+H]⁺, calcd for C₃₄H₄₇O₅. ¹H and ¹³C NMR data; see Tables SI1 and SI10 (Supplementary Information).

3β-O-(3'-Methoxybenzoyl)-5α,25R-spirostan-12-one (3)

General esterification procedure using 2-methoxybenzoyl chloride afforded **3** in a 70% yield as a white amorphous powder. TLC: *n*-hexane-acetone, 7:3; ESI-MS *m/z*: 565.3 [M+H]⁺, calcd for C₃₅H₄₉O₆. ¹H and ¹³C NMR data; see Tables SI1 and SI10 (Supplementary Information).

3β-O-(3'-Chlorobenzoyl)-5α,25R-spirostan-12-one (4)

General esterification procedure using 2-chlorobenzoyl chloride afforded **4** in a 60% yield as a white amorphous powder. TLC: *n*-hexane-acetone, 7:3; ESI-MS *m/z*: 569.5 [M+H]⁺, calcd for C₃₄H₄₆ClO₅. ¹H and ¹³C NMR data; see Tables SI1 and SI10 (Supplementary Information).

3β-O-(Furoyl)-5α,25R-spirostan-12-one (5)

General esterification procedure using 2-furoyl chloride afforded **5** in 71% yield as a white amorphous powder, TLC: *n*-hexane-acetone, 7:3; ESI-MS *m/z*: 525.3 [M+H]⁺ calcd for C₃₂H₄₅O₆. ¹H and ¹³C NMR data; see Tables SI2 and SI11 (Supplementary Information).

3β-O-(4'-Trifluoromethylbenzoyl)-5α,25R-spirostan-12-one (6)

General esterification procedure using 3-trifluoromethyl benzoyl chloride afforded **6** in a 55% yield as a white amorphous powder. TLC: *n*-hexane-acetone, 7:3; ESI-MS *m/z*: 603.3 [M+H]⁺, calcd for C₃₅H₄₆F₃O₅. ¹H and ¹³C NMR data; see Tables SI1 and SI10 (Supplementary Information).

3β-O-(5'-Fluorobenzoyl)-5α,25R-spirostan-12-one (7)

General esterification procedure using 4-fluorobenzoyl chloride afforded **7** in 35% yield as white amorphous powder, TLC: *n*-hexane:acetone, 7:3; ESI-MS *m/z*: 553.7 [M+H]⁺ calcd for C₃₄H₄₆FO₅. ¹H and ¹³C NMR data; see Tables SI2 and SI10 (Supplementary Information).

3β-O-(5'-Cyanobenzoyl)-5α,25R-spirostan-12-one (8)

General esterification procedure using 4-cyanobenzoyl chloride afforded **8** in 68% yield as white amorphous powder, TLC: *n*-hexane:acetone, 7:3; ESI-MS *m/z*: 560.3 [M+H]⁺ calcd for C₃₅H₄₆NO₅. ¹H and ¹³C NMR data; see Tables SI2 and SI10 (Supplementary Information).

3β-O-(5'-Nitrobenzoyl)-5α,25R-spirostan-12-one (9)

General esterification procedure using 4-nitrobenzoyl chloride afforded **9** in a 63% yield as a white amorphous powder, TLC: *n*-hexane:acetone, 7:3; ESI-MS *m/z*: 580.3 [M+H]⁺ calcd for C₃₄H₄₆NO₇. ¹H and ¹³C NMR data; see Tables SI2 and SI11 (Supplementary Information).

Preparation of 3-O-hecogenin-12-phenyl semicarbazones and phenylthiosemicarbazones**General procedure A**

A solution of hecogenin (20 mg, 0.046 mmol) in dry EtOH (5 mL) and pyridine (0.5 mL) mixture, was charged with three equivalents of appropriate functionalized phenyl semicarbazide.HCl or phenyl thiosemicarbazide.HCl. The resulting mixture was stirred overnight at RT. The mixture was diluted with ice-cold water and the precipitate formed was filtered and washed with ice cold water (2 x 5 mL) after reaction completion. The combined solid was lyophilized and then solubilized in EtOAc. The crude product was purified by flash column chromatography using Si gel 60 eluted with gradients of *n*-hexanes-EtOAc (8:2 to 6:4), to afford the corresponding hecogenin 12-semicarbazones or thiosemicarbazones.

3β-Hydroxy-5α,25R-spirostan-12-(phenyl-semicarbazone) (10)

General condensation procedure A, using 4-(phenyl)-3-semicarbazide.HCl afforded **10** in 30% yield as white amorphous powder, TLC: *n*-hexane-acetone-NH₃, 7:3:0.5; ESI-MS *m/z*: 564.7 [M+H]⁺ calcd for C₃₄H₅₀N₃O₄. ¹H and ¹³C NMR data; see Tables SI3 and SI11 (Supplementary Information).

3β-Hydroxy-5α,25R-spirostan-12-(4'-chlorophenyl semicarbazone) (**11**)

General reaction procedure A using 4-(3-chlorophenyl)-3-semicarbazide.HCl afforded **11** in 46% yield as a white amorphous powder, TLC: *n*-hexane-acetone-NH₃, 7:3:0.5; ESI-MS *m/z*: 598.4 [M+H]⁺, calcd for C₃₄H₄₉ClN₃O₄. ¹H and ¹³C NMR data; see Tables SI3 and SI11 (Supplementary Information).

3β-Hydroxy-5α,25R-spirostan-12-(5'-chlorophenyl semicarbazone) (**12**)

General reaction procedure A using 4-(4-chlorophenyl)-3-semicarbazide.HCl afforded **12** in 40% yield as a white amorphous powder, TLC: *n*-hexane-acetone-NH₃, 7:3:0.5; ESI-MS *m/z*: 598.4 [M+H]⁺ calcd for C₃₄H₄₉ClN₃O₄. ¹H and ¹³C NMR data; see Tables SI3 and SI11 (Supplementary Information).

3β-Hydroxy-5α,25R-spirostan-12-(4'-trifluoromethylphenyl semicarbazone) (**13**)

General reaction procedure A using 4-(3-trifluoromethylphenyl)-3-semicarbazide.HCl afforded **13** in 37% yield as a white amorphous powder, TLC: *n*-hexane-acetone-NH₃, 7:3:0.5; ESI-MS *m/z*: 632.4 [M+H]⁺ calcd for C₃₅H₄₉F₃N₃O₄. ¹H and ¹³C NMR data; see Tables SI3 and SI11 (Supplementary Information).

3β-Hydroxy-5α,25R-spirostan-12-[(5'-methylphenylsulphonyl)semicarbazone] (**14**)

General reaction procedure A using 4-(4-methylphenylsulfonyl)-3-semicarbazide.HCl afforded **14** in 52% yield as a white amorphous powder, TLC: *n*-hexane-acetone-NH₃, 7:3:0.5;

ESI-MS m/z : 642.6 $[M+H]^+$ calcd for $C_{35}H_{52}N_3O_6S$. 1H and ^{13}C NMR data; see Tables SI3 and SI12 (Supplementary Information).

General procedure B

Hecogenin (20 mg, 0.046 mmol) was dissolved in dry EtOH (5 mL) and pyridine (0.5 mL) mixtures, and then charged with three equivalents of appropriate phenyl semicarbazide or phenyl thiosemicarbazide. The resulting mixture was stirred overnight at room temperature. Water was added to quench the reaction and the product was extracted with EtOAc (3 x 5L) after reaction completion. The combined organic layers dried were dried over anhydrous Na_2SO_4 and concentrated under vacuum. The crude residue was purified using flash column chromatography over silica gel 60, eluted with gradients of *n*-hexanes-EtOAc- NH_4OH (8:2:0.5 to 6:4:0.5), to afford the corresponding hecogenin 12-phenyl semicarbazones or phenyl thiosemicarbazones.

3 β -Hydroxy-5 α ,25R-spirostan-12-(phenyl thiosemicarbazone) (**15**)

General reaction procedure B using 4-phenyl thiosemicarbazide, afforded **15** in 78% yield as a white amorphous powder, TLC: *n*-hexane-acetone- NH_3 , 7:3:0.5; ESI-MS m/z : 580.3 $[M+H]^+$ calcd for $C_{34}H_{50}N_3O_3S$. 1H and ^{13}C NMR data; see Tables SI4 and SI12 (Supplementary Information).

3 β -Hydroxy-5 α ,25R-spirostan-12-(3'-chlorophenyl thiosemicarbazone) (**16**)

General reaction procedure B using 4-(2-chlorophenyl)-3-thiosemicarbazide afforded **16** in 65% yield as a white amorphous powder, TLC: *n*-hexane-acetone- NH_3 , 7:3:0.5; ESI-MS m/z : 614.5 $[M+H]^+$ calcd for $C_{34}H_{49}ClN_3O_3S$. 1H and ^{13}C NMR data; see Tables SI4 and SI12 (Supplementary Information).

3 β -Hydroxy-5 α ,25R-spirostan-12-(5'-chlorophenyl thiosemicarbazone) (**17**)

General reaction procedure B using 4-(4-chlorophenyl)-3-thiosemicarbazide afforded **17** in 46% yield as a white amorphous powder, TLC: *n*-hexane-acetone-NH₃, 7:3:0.5; ESI-MS *m/z*: 614.5 [M+H⁺] calcd for C₃₄H₄₉ClN₃O₃S. ¹H and ¹³C NMR data; see Tables SI4 and SI12 (Supplementary Information).

3β-Hydroxy-5α,25R-spirostan-12-(3',5'-dichlorophenyl thiosemicarbazone) (**18**)

General reaction procedure B using 4-(2,4-dichlorophenyl)-3-thiosemicarbazide afforded **18** in 58% yield as a white amorphous powder, TLC: *n*-hexane-acetone-NH₃, 7:3:0.5; ESI-MS *m/z*: 648.3 [M+H⁺] calcd for C₃₄H₄₈Cl₂N₃O₃S. ¹H and ¹³C NMR data; see Tables SI5 and SI12 (Supplementary Information).

3β-Hydroxy-5α,25R-spirostan-12-(3',7'-dichlorophenyl thiosemicarbazone) (**19**)

General reaction procedure B using 4-(2,6-dichlorophenyl)-3-thiosemicarbazide afforded **19** in 45% yield as a white amorphous powder, TLC: *n*-hexane-acetone-NH₃, 7:3:0.5; ESI-MS *m/z*: 648.3 [M+H⁺] calcd for C₃₄H₄₈Cl₂N₃O₃S. ¹H and ¹³C NMR data; see Tables SI5 and SI12 (Supplementary Information).

3β-Hydroxy-5α,25R-spirostan-12-(5'-fluorophenyl thiosemicarbazone) (**20**)

General reaction procedure B using 4-(4-fluorophenyl)-3-thiosemicarbazide afforded **20** in 30% yield as a white amorphous powder, TLC: *n*-hexane-acetone-NH₃, 7:3:0.5; ESI-MS *m/z*: 598.3 [M+H]⁺ calcd for C₃₄H₄₉FN₃O₃S. ¹H and ¹³C NMR data; see Tables SI5 and SI12 (Supplementary Information).

3β-Hydroxy-5α,25R-spirostan-12-(3'-nitrophenyl thiosemicarbazone) (**21**)

General reaction procedure B using 4-(2-nitrophenyl)-3-thiosemicarbazide afforded **21** in 72% yield as a yellow amorphous powder, TLC: R_f=0.25 (*n*-hexane-acetone-NH₃, 7:3:0.5); ESI-

MS m/z : 625.3 $[M+H]^+$ calcd for $C_{34}H_{49}N_4O_5S$. 1H and ^{13}C NMR data; see Tables SI5 and SI13 (Supplementary Information).

3 β -Hydroxy-5 α ,25R-spirostan-12-(5'-nitrophenyl thiosemicarbazone) (**22**)

General reaction procedure Busing 4-(4-nitrophenyl)-3-thiosemicarbazide afforded **22** in 45% yield as a yellow amorphous powder, TLC: *n*-hexane-acetone-NH₃, 7:3:0.5; ESI-MS m/z : 625.3 $[M+H]^+$ calcd for $C_{34}H_{49}N_4O_5S$. 1H and ^{13}C NMR data; see Tables SI6 and SI13 (Supplementary Information).

3 β -Hydroxy-5 α ,25R-spirostan-12-(3'-trifluoromethylphenyl thiosemicarbazone) (**23**)

General reaction procedure Busing 4-(2-trifluoromethylphenyl)-3-thiosemicarbazide afforded **23** in 75% yield as a white amorphous powder, TLC: *n*-hexane-acetone-NH₃, 7:3:0.5; ESI-MS m/z : 648.7 $[M+H]^+$ calcd for $C_{35}H_{49}F_3N_3O_3S$. 1H and ^{13}C NMR data; see Tables SI6 and SI13 (Supplementary Information).

3 β -Hydroxy-5 α ,25R-spirostan-12-(5'-trifluoromethylphenyl thiosemicarbazone) (**24**)

General reaction procedure Busing 4-(4-trifluoromethylphenyl)-3-thiosemicarbazide, afforded **24** in 50% yield as a white amorphous powder, TLC: *n*-hexane-acetone-NH₃, 7:3:0.5; ESI-MS m/z : 648.7 $[M+H]^+$ calcd for $C_{35}H_{49}F_3N_3O_3S$. 1H and ^{13}C NMR data; see Tables SI6 and SI13 (Supplementary Information).

3 β -Hydroxy-5 α ,25R-spirostan-12-(4',6'-di-trifluoromethylphenylthiosemicarbazone) (**25**)

General reaction procedure Busing 4-(3,5-difluoromethylphenyl)-3-thiosemicarbazide afforded **25** in 35% yield as a white amorphous powder, TLC: *n*-hexane-acetone-NH₃, 7:3:0.5; ESI-MS m/z : 716.3 $[M+H]^+$ calcd for $C_{36}H_{48}F_6N_3O_3S$. 1H and ^{13}C NMR data; see Tables SI6 and SI13 (Supplementary Information).

3 β -Hydroxy-5 α ,25R-spirostan-12-(3'-methoxyphenyl thiosemicarbazone) (**26**)

General reaction procedure Busing 4-(2-methoxyphenyl)-3-thiosemicarbazide afforded **26** in 56% yield as a white amorphous powder, TLC: *n*-hexane-acetone-NH₃, 7:3:0.5; ESI-MS *m/z*: 625.3 [M+H]⁺ calcd for C₃₅H₅₂N₃O₄S. ¹H and ¹³C NMR data; see Tables SI7 and SI14 (Supplementary Information).

3β-Hydroxy-5α,25R-spirostan-12-(5'-methoxyphenyl thiosemicarbazone) (27)

General reaction procedure Busing 4-(4-methoxyphenyl)-3-thiosemicarbazide afforded **27** in 45% yield as a white amorphous powder, TLC: *n*-hexane-acetone-NH₃, 7:3:0.5; ESI-MS *m/z*: 625.3 [M+H]⁺ calcd for C₃₅H₅₂N₃O₄S. ¹H and ¹³C NMR data; see Tables SI7 and SI14 (Supplementary Information).

3β-Hydroxy-5α,25R-spirostan-12-(5'-phenoxyphenyl thiosemicarbazone) (28)

General reaction procedure Busing 4-(4-phenoxyphenyl)-3-thiosemicarbazide afforded **37** in 25% yield as a white amorphous powder, TLC: R_f=0.20 (*n*-hexane-acetone-NH₃, 7:3:0.5); ESI-MS *m/z*: 672.3 [M+H]⁺ calcd for C₄₀H₅₄N₃O₄S. For ¹H and ¹³C NMR data of **28**, see Tables SI7 and SI14 in Supplementary Information.

3β-Hydroxy-5α,25R-spirostan-12-(3'-ethylphenyl thiosemicarbazone) (29)

General reaction procedure Busing 4-(2-ethylphenyl)-3-thiosemicarbazide afforded **29** in 35% yield as a white amorphous powder, TLC: *n*-hexane-acetone-NH₃, 7:3:0.5; ESI-MS *m/z*: 608.5 [M+H]⁺ calcd for C₃₆H₅₄N₃O₃S. ¹H and ¹³C NMR data; see Tables SI7 and SI14 (Supplementary Information).

3β-Hydroxy-5α,25R-spirostan-12-(3'-methylphenyl thiosemicarbazone) (30)

General reaction procedure Busing 4-(2-methylphenyl)-3-thiosemicarbazide afforded **30** in 75% yield as a yellowish white amorphous powder, TLC: *n*-hexane-acetone-NH₃, 7:3:0.5;

ESI-MS m/z : 594.9 $[M+H]^+$ calcd for $C_{35}H_{52}N_3O_3S$. 1H and ^{13}C NMR data; see Tables SI7 and SI14 (Supplementary Information).

3 β -Hydroxy-5 α ,25R-spirostan-12-(5'-methylphenyl thiosemicarbazone) (31)

General reaction procedure Busing 4-(4-methylphenyl)-3-thiosemicarbazide afforded **31** in 35% yield as a white amorphous powder, TLC: *n*-hexane-acetone-NH₃, 7:3:0.5; ESI-MS m/z : 594.9 $[M+H]^+$ calcd for $C_{35}H_{52}N_3O_3S$. 1H and ^{13}C NMR data; see Tables SI8 and SI14 (Supplementary Information).

3 β -Hydroxy-5 α ,25R-spirostan-12-(3',5'-dimethylphenyl thiosemicarbazone) (32)

General reaction procedure Busing 4-(2,4-dimethylphenyl)-3-thiosemicarbazide afforded **32** in 30% yield as a white amorphous powder, TLC: *n*-hexane-acetone-NH₃, 7:3:0.5; ESI-MS m/z : 608.5 $[M+H]^+$ calcd for $C_{36}H_{54}N_3O_3S$. 1H and ^{13}C NMR data; see Tables SI8 and SI15 (Supplementary Information).

3 β -Hydroxy-5 α ,25R-spirostan-12-(3',7'-dimethylphenyl thiosemicarbazone) (33)

General reaction procedure Busing 4-(2,6-dimethylphenyl)-3-thiosemicarbazide afforded **33** in 25% yield as a white amorphous powder, TLC: *n*-hexane-acetone-NH₃, 7:3:0.5; ESI-MS m/z : 608.5 $[M+H]^+$ calcd for $C_{36}H_{54}N_3O_3S$. 1H and ^{13}C NMR data; see Tables SI8 and SI15 (Supplementary Information).

3 β -Hydroxy-5 α ,25R-spirostan-12-(4',5'-methylenedioxyphenyl thiosemicarbazone) (34)

General reaction procedure Busing 4-(3,4-methylenedioxyphenyl)-3-thiosemicarbazide afforded **35** in 30% yield as a white amorphous powder, TLC: *n*-hexane-acetone-NH₃, 7:3:0.5; ESI-MS m/z : 624.3 $[M+H]^+$ calcd for $C_{35}H_{50}N_3O_5S$. 1H and ^{13}C NMR data; see Tables SI8 and SI15 (Supplementary Information).

Molecular modeling

In silico experiments were implemented on iMac27-inch Z0PG workstation (Apple, Cupertino, CA, USA) equipped with 3.5 GHz Intel Core i7 processor with 16 GB 1600 MHz DDR3 memory module operated under OS X software (version 10.9.5).

Ligand preparation

Ligands structure delineated using the 2D sketcher wizard in Maestro 9.3 panel (Maestro, version 9.3, 2012, Schrödinger, New York, NY, USA). Replaced workstation was applied for 3D structure transformation. Calculations for low energy 3D ligands structure were implemented using the default job settings of LigPrep 2.3 module (LigPrep, version 2.3, 2012, Schrödinger, New York, NY, USA). Structures were imported and their conformations energy was minimized using the optimized potential for liquid simulations (OPLS-2005, Schrödinger, New York, NY, USA) force field and nearby 32 conformations per ligands were generated. Tautomeric and ionization states were generated using Epik at target $\text{pH}=7.0 \pm 2$.

Protein preparation

The X-ray structure of the human mitogen-activated protein kinase (MAPK), UNP residues 35-393) in a binary complex with competitive inhibitor (K252A) and MG2P imported typically from RCSB Protein Data Bank (PDB code 3EQF) to Maestro Workspace [42]. The Protein Preparation Wizard of the Schrödinger suite was implemented to prepare MEK kinase domain. Protein was pre-processed by assigning bond orders, added hydrogen, filled in the missing loops and the side chains using Prime. Water molecules were deleted beyond 5 Å from the ligand and ionization/tautomeric states were generated at $\text{pH } 7.0 \pm 3.0$ using Epik. Hydrogen bonds were assigned for protein refinement. Docking grids were generated by Glide-docking using the default value of the protein atomic scale (1.0 Å) within the cubic box centered on the co-crystallized ligand.

Ligand docking

Docking calculations were accomplished using Glide 5.8 module³² in standard (XP) mode.⁴³ Ligands were docked flexibly by using penalization for non-planar amide bond conformations.

In vitro activities

Cell lines and culture conditions

The MDA-MB-231, MDA-MB-468, MCF-10A, MCF-7, T-47D, BT-474 and SKBR-3 human mammary cell lines were obtained from the American Type Culture Collection (ATCC, Manassas, VA, USA). Breast cancer MDA-MB-231/Green Florescent Protein-tagged (MDA-MB-231/GFP) cell line was purchased from Cell Biolabs (San Diego, CA, USA). Cells were used after thawed with periodic recording of morphology and doubling times to ensure maintenance of phenotype and maintained at 37°C under humidified atmosphere of 5% CO₂ in their specific medium according to the supplier's instructions. MDA-MB-231 and MDA-MB-468 breast cancer cells were grown in Rosselle's Park Memorial Institute medium (RPMI-1640; Corning, Manassas, VA, USA) supplemented with 10% heat-inactivated FBS (Hyclone, Salt Lake City, UT, USA) and 1% penicillin/streptomycin (InvitrogenTM, Carlsbad, CA, USA). ER_α expressing, breast cancer cell lines were grown in Dulbecco's modified Eagle's medium (DMEM; Gibco[®] by Life Technologies, Grand Island, NY, USA) supplemented with 10% hyclone fetal bovine serum (GE Healthcare Life Sciences, Pittsburgh, PA, USA). The immortalized, mammary epithelial MCF-10A cells were maintained in DME/high glucose medium (Gibco[®] Life Technologies, Grand Island, NY, USA) supplemented with 10 % horse serum (Gibco[®] by Life Technologies, Grand Island, NY), 20 ng/mL EGF (Peprotech, Rocky Hill, NJ, USA), 0.5 mg/mL hydrocortisone, 100 ng/mL cholera toxin and 10 μg/mL insulin. All

cell-based assays were performed using cells in the exponential growth phase. Tested compounds were dissolved in biological grade, sterile dimethyl sulfoxide (DMSO) (Invitrogen™) as 10 mM stock solution and kept at -20°C. The drug was diluted in culture media just prior treatment and used at various concentrations as indicated. Oleanolic acid (10 μM)⁴⁴ was used as a positive drug control, while DMSO as vehicle negative control.

Proliferation assay

Cell proliferation was measured using MTT (3-(4,5-dimethylthiazol-2-yl)-2,5-diphenyltetrazolium bromide) cell reduction assay, according to the manufacturer's protocol. Briefly, cells were seeded at density of 8×10^3 cells/well in 96-well flat bottom plates each in its defined growth medium and allowed to attach overnight prior to treatment exposure. In the next day, media were replaced by fresh ones containing different concentrations of analogs **1-34** for 72 h. A matched control cell standard curve using sequentially increased cell numbers was included for each corresponding cell line to determine growth inhibition. At the end of incubation period, media were gently aspirated and cells were rinsed with PBS. Thereafter, 100 μL of fresh media and 50 μL of MTT solution were added to each well. Cells were then incubated for additional 3 h. Supernatants were carefully removed and formazan crystals were dissolved in 100 μL DMSO. The absorbance was read at 570 nm on a Synergy™ 4 Multi-Mode Microplate Reader and analyzed with Gen5™ Data Analysis Software (BioTek, Winooski, VT, USA). Data are represented as mean percent cell survival \pm SEM of triplicate experiments. Percent cell survival was calculated as follows: % cell survival = (Cell No._{treatment}/Cell No._{DMSO}) x 100.

Cytotoxicity assay

The human, non-tumorigenic, mammary epithelial MCF-10A cells were used to assess the selectivity of analogue **30**. The confluent monolayer of cells were harvested and seeded into 96-well plate at density 3×10^4 cells/well. Cells allowed attaching overnight at 37 °C in 5% CO₂ humidified incubator. Cells were then treated with **30** at different concentrations in fresh serum-free media or DMSO as vehicle control, after which incubation was resumed at 37 °C in humidified atmosphere of 5% CO₂. At the end of treatment period, media were replaced by fresh ones containing 50 µL MTT (1 mg/mL in PBS) and incubated for further 3 h. The insoluble, fully grown formazan crystals were dissolved in 100 µL of DMSO with gentle tapping and absorbance was measured at 570 nm on Synergy2 BioTek™ microplate reader (BioTek® Instruments Inc., Winooski, VT, USA). The average of triplicate readings was considered and number of cells per well was calculated from the standard curve prepared by plating various cell concentrations (5000-60,000 cells per well), at the start of the experiment. Percent cell viability was calculated by the previously stated formula in proliferation assays.

Lactate dehydrogenase (LDH) release assay

The Cayman's lactate dehydrogenase (LDH) based cytotoxicity kit (Cayman, Ann Arbor, MI, USA) was used to measure cancer cellular death in response to **1** or **30** treatments. In brief, MDA-MB-231 cells were seeded into 96-well plate at a cell density of 3×10^4 cells/well in 200 µL culture medium. Equal volume of culture medium was added to three wells as background control. After cell attachment, media were removed and cells were treated with 200 µL of 5% serum culture media containing **1** (25-100 µM) or **30** (1.2-10.0 µM) in triplicates. Triton X-100 (20 µL, 10%) solution was added to three wells containing the cells and assigned as high release control and 20 µL of assay buffer to other three cell-free wells which assigned as low release control. The microplate was then incubated for 24 h. Plate was centrifuged for five minutes and

100 μL of cell supernatant were transferred to a new 96-well plate. Reaction buffer (100 μL of NAD^+ , lactic acid, INT, reconstituted diaphorase) was added to each well and the plate placed on an orbital shaker for 30 minutes at room temperature. Finally, absorbance was measured at 490 nm using BioTek Synergy 2 microplate reader (BioTek[®] Instruments Inc., Winooski, VT, USA). Percent cytotoxicity was calculated by substituting the resulting absorbance values into the following formula:

$$\% \text{ Cytotoxicity} = \left[\frac{(\text{Treatment Abs}) - (\text{Low control Abs})}{(\text{High control Abs}) - (\text{Low control Abs})} \right] \times 100$$

Migration assay

The scratch wound healing assay (WHA) was implemented to screen the migration suppressing effect of various concentrations of **1** and **30** against the invasive TNBC MDA-MB-231 cells following the procedure previously described.⁴⁴ Briefly, cells were harvested and plated in sterile 24-well plate then allowed overnight to recover and attach. In the next day, a scratch wound was inflicted in the confluent monolayer per each well using a sterile 200 μL pipette tip. Media were aspirated; cells were washed twice with PBS then re-incubated in serum-free media for 4 h. Subsequently, media were replaced by fresh serum free media supplemented with the scattering factor (HGF, 100 ng/mL) and different concentrations of **1** or **30**. Incubation was resumed till wound was just about to close in control wells. Media was then aspirated, cells were fixed using cold ethanol and images were captured for each wound. Percent migrated cells were determined using the following formula:

$$(\%) \text{ Percent migration} = \frac{\text{wound width at zero time} - \text{wound width in treated well}}{\text{wound width at zero time} - \text{wound width in DMSO}} \times 100$$

Invasion assay

The anti-invasive capacity of **1** and **30** against the invasive MDA-MB-231 cells was assessed using the CultreCoat[®] 96-well BME Cell Invasion Assay kit (Trevigen[®], Gaithersburg, MD, USA) in accordance with the vendor's protocol.⁴⁵ The 96-well invasion chamber was rehydrated by adding 25 μ L of warm serum free RPMI-1640 media and incubated at 37 °C for 1 h. To each top chamber was added 25 μ L of cell suspension/well (1×10^6 cells/mL), while 150 μ L of serum-free media supplemented with 100 ng/mL HGF and **1** (10-80 μ M) or **30** (0.6-5 μ M) was added to bottom chambers. Plates were then assembled and incubated overnight. Thereafter, media were aspirated from top chamber, washed with washing buffer and transferred to the receiver plate. About 100 μ L of cell dissociation solution/calcein-AM was added to each of lower chamber wells and incubation resumed for 1h. Fluorescence of the lower plate was measured at 485 nm excitation, 520 nm emission on a BioTek Synergy 2 microplate reader (BioTek[®] Instruments Inc., Winooski, VT, USA). The number of cells invaded per well was calculated against a standard curve prepared by plating various numbers of cells. Percent invasion was calculated relative to vehicle control wells as previously reported^{46, 47} and IC₅₀ value was calculated using GraphPad Prism version 5.01 (GraphPad Software, San Diego, CA, USA).

Protein extraction and immunoblotting

The human breast cancer MDA-MB-231 cells were seeded at a density of 5×10^5 /100 mm culture dish and incubated overnight to recover and attach. Cells were treated either with **1**, **30** or DMSO as vehicle control in serum reduced media (supplemented with 100 ng/ml HGF for c-Met dependent MDA-MB-231 cells) for 72 h. Total cellular protein contents were obtained using RIPA Lysis and Extraction Buffer (Thermo Fisher Scientific, Madison, WI, USA) supplemented

with mammalian protease arrest (G-Biosciences, St. Louis, MO, USA). Samples were diluted in Laemmli buffer (BIO-RAD, Hercules, CA) containing 5% β -mercapto ethanol (Sigma-Aldrich, St. Louis, MO, USA) prior loading on gels. Cell lysates (30 μ g) were electrophoresed on Mini-PROTEAN[®] TGX[™] precast polyacrylamide gels (BIO-RAD, Hercules, CA, USA) using Tris/Glycine/SDS running buffer and then transferred to Immuno-Blot[®] PVDF membranes (BIO-RAD, Hercules, CA, USA). Blotted membranes were then blocked with 5% BSA (Cell Signaling Technology, Beverly, MA, USA) in TBST (10 mM Tris-HCl, 150 mM NaCl, 0.1% Tween-20) for 2 h with gentle agitation at room temperature. Immunoblots were incubated overnight at 4 °C with appropriate primary antibodies (Cell Signaling Technology, Beverly, MA). After incubation, membranes were washed three times with TBST and then incubated with HRP-labeled secondary antibodies (Cell Signaling Technology, Beverly, MA, USA) for 1 h with agitation at room temperature. Chemiluminescence detection was performed using Super Signal West Pico kit (Thermo Fisher Scientific, Madison, WI, USA) and G. BOX imaging system with high resolution 100m pixel camera (Syngene, Fredrick, MD, USA).

***In vivo* study**

Animals

Female athymic Foxn1^{nu}/Foxn1⁺ mice aged 7-9 weeks, with average body weight of 19-23 g were purchased from Harlan (Indianapolis, IN, USA) and hosted in the pathogen-free animal facility at School of Pharmacy, University of Louisiana at Monroe. The mice housed in four per laminar flow cabinets spread with loose pulp Alpha-Dri[™] bedding. Pellets of standard Teklad rodent chow (Madison, WI, USA) and water were available *ad libitum* throughout the study periods. Fluorescent lighting was controlled automatically to provide alternate light/dark cycles of 12 h each. Temperature and humidity were centrally controlled at 23 \pm 2 °C of 55 \pm 5%

relative humidity. All animals were observed and examined for general health for one-week prior the study initiation. Strict animal care procedures set forth by the Institutional Animal Care and Use Committee based on the NIH guidelines for the care and the standards of the Institutional Animal Care and Use Committee, University of Louisiana at Monroe (IACUC) were strictly followed.

Orthotopic xenograft model

MDA-MB-231/GFP human breast cancer cells were harvested, centrifuged and cell pellet washed twice with sterile PBS and resuspended in RPMI-1640 serum-free medium such that 1×10^6 cells suspended in 20 μ L media. Cell suspension (20 μ L) was injected into the 2nd mammary gland fat pad just beneath the nipple per mouse on day zero of the study to induce an orthotopic primary tumor xenograft. Once tumors became palpable (average volume of 50 mm³), mice were randomized and assigned to control and treatment groups (4 mice/group). The control group administered 2% DMSO/PBS as a vehicle. The treatment group I received hecogenin (**1**) *ip* at 10 mg/kg dose regimens, 3X/week, while treatment group II received **30** at the same dose, 3X/ week/ *ip*. All treatments solution was freshly prepared on the dosing day as a stock of 1 mg/20 μ L DMSO then diluted with sterile PBS containing 0.1% Tween 80 to the required final volume. Sterile insulin syringes U-100 (29G x 0.5cc) were used for injections. Tumor dimensions were assessed with each dosing using an electronic digital calliper (Traceable[®], VWR, Radnor, PA, USA). Tumor volume (TV, mm³) was calculated using calliper measurements of tumor dimensions in mm using the formula for a prolate ellipsoid: $[(\text{length} \times \text{width}^2)/2]$. Body weight (BW) was recorded every other day by placing each mouse in a pre-weighted plastic container on a digital scale (VWR, USA). The study ended on the 33rd day, once the calculated TV of the control group reached its maximum animal burden ($\text{TV}_c >$

10% BW, $\sim 2 \text{ cm}^3$). All mice were then anesthetized using ketamine/xylazine combination to relief ketamine's induced muscle rigidity and twitching. The mixture was prepared as ketamine (100 mg/mL)-xylazine (10 mg/mL)-isotonic saline in a ratio of 1: 0.5: 8.5, respectively, and administrated to mice at a dose of $10 \mu\text{L/g/i.p.}$ which is sufficient for 20 min trance-like state. Thereafter, mice were euthanized by cervical dislocation, tumors were excised, weighed and tumor tissue sample was snap frozen in liquid nitrogen and stored at -80°C . Since tumors were established and well detected before the treatment initiation, hence this volume was deducted while calculating final percentage tumor growth inhibition from the formula as: $100 \times \{1 - [(TV_T - TV_0)/(TV_C - TV_0)]\}$. TV_T =tumor volume of treatment groups at the study end, TV_0 =tumor volume of control group at the start of the study. TV_C = tumor volume of control group at the study end.

Statistics

The results were presented as the means \pm SEM of at least three independent experiments. Pooled data were subjected to statistical analyses using GraphPad Prism version 5.01 (GraphPad Software, CA). Differences between means from two different groups were subjected to student's 't' test, whereas one-way analysis of variance (ANOVA) was used to analyze significant differences between three or more groups. The *In vivo* tumor growth data were subjected to two-tailed student's 't' test. A difference of $p < 0.05$ was considered statistically significant as compared to the vehicle-treated control group and indicated by asterisk (*). The IC_{50} values were determined using a non-linear regression curve fitting analysis using GraphPad Prism software version 5 (La Jolla, CA, USA).

Acknowledgements

The Egyptian Ministry of Higher Education is acknowledged for supporting H.E. Elsayed's fellowship.

Supplementary data

Supplementary data associated with this article including: Tables S11-15, ^1H and ^{13}C NMR data of analogs **2-34** can be found in the online version

References and notes

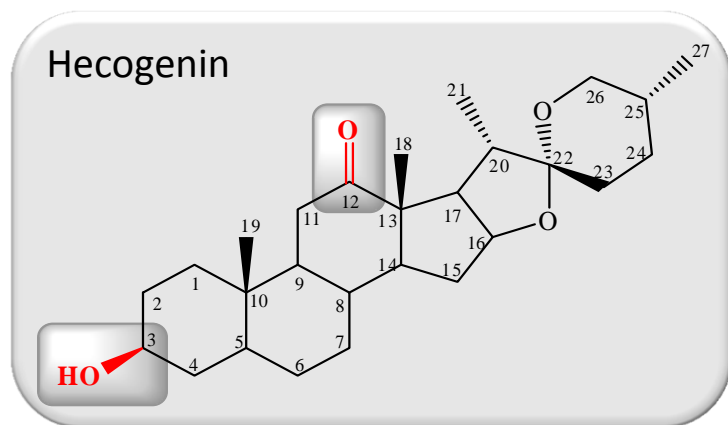
1. Fernandez-Herrera, M.A.; Sandoval-Rairez, J.; Meza-Reyes, S.; Montiel-Smith, S. *J. Mex. Chem. Soc.* **2009**, *53*, 126-130.
2. Gama, K.B.; Quintans, J.S.S.; Antonioli, A.R.; Quintans-Junior, L.J.; Santana, W.A.; Branco, A.; Soares, M.B.P.; Villarreal, C.F. *J. Nat. Prod.* **2013**, *76*, 559-563.
3. Corbiere, C.; Liagre, B.; Bianchi, A.; Bordji, K.; Dauca, M.; Netter, P.; Beneytout, J. *Int. J. Oncol.* **2003**, *22*, 899-905.
4. Cerqueira, G.S.; Silva, G.D.S.; Vasconcelos, E.R.; Freitas, A.P.F.; Moura, B.A.; Macedo, D.S.; Souto, A.L.; Filho, J.M.B.; Leal, L.K.L.; Brito, G.A.C.; Souccar, C.; Viana, G.S.B. *Eur. J. Pharmacol.* **2012**, *683*, 260-269.
5. Peana, A.T.; Moretti, M.D.; Manconi, V.; Desole, G.; Pippia, P. *Planta Med.* **1997**, *63*, 199-202.
6. Díaz, A.C.; Pablo Garcia Merinos, J.; López, Y.; Betzabe González Campos J.; de Río, R. E.; Santillan, R.; Farfán, N.; Morzycki, J.W. *Steroids* **2015**, *100*, 36-43.

7. Fernández-Herrera, M.A.; López-Muñoz, H.; Hernández-Vázquez, J.M.V.; López-Dávila, M.; Escobar-Sánchez, M.L.; Sánchez-Sánchez, L.; Pinto, B.M.; Sandoval-Ramírez, J. *Bioorg. Med. Chem.* **2010**, *18*, 2474-2484.
8. Gryszkiewicz-Wojtkielewicz, A.; Jastrzebska, I.; Morzycki, J.W.; Romanowska, D.B. *Curr. Org. Chem***2003**, *7*, 1-22.
9. Ravindar, K.; Reddy, M.S.; Lindqvist, L.; Pelletier, J.; Deslongchamps, P. *J. Org. Chem.* **2011**, *76*, 1269-1284.
10. Gasparotto, J.; Somensi, N.; Kunzler, A.; Girardi, C. S.; de BittencourtPasquali, M. A.; Ramos, V. M.; Simoes-Pires, A.; Quintans-Junior, L. J.; Branco, A.; Moreira, J. C.; Gelain, D. P. *Anticancer Agents Med. Chem.***2014**, *14*,1128-1135.
11. Shipman, J.C.; Smith, S.H.; Drach, J.C.; Klayman, D.L. *Antimicrob. Agents. Chemother.* **1981**, *19*, 682-685.
12. Siddiqui, N.; Singh, O. *Indian J. Pharm. Sci.* **2003**, *65*, 423-425.
13. Chipeleme, A.; Gut, J.; Rosenthal, B.P.J.; Chibale, K. *Bioorg. Med. Chem.* **2007**, *17*, 6434-6438.
14. Yuan, J.; Lovejoy, D.B.; Richardson, D.R. *Blood.* **2004**, *104*, 1450-1458.
15. Brockman, R.W.; Sidwell, R.W.; Arnett, G.; Shaddix, S. *Proc. Soc. Exp. Biol. Med.* **1970**, *133*, 609-614.
16. Hall, I.H.; Lackey, C.B.; Kistler, T.D.; Jr Durham, R.W.; Jouad, E.M.; Khan, M.; Thanh, X.D.; Djebbar-Sid, S.; Benali-Baitich, O.; Bouet, G.M. *Pharmazie.* **2000**, *55*, 937-941.

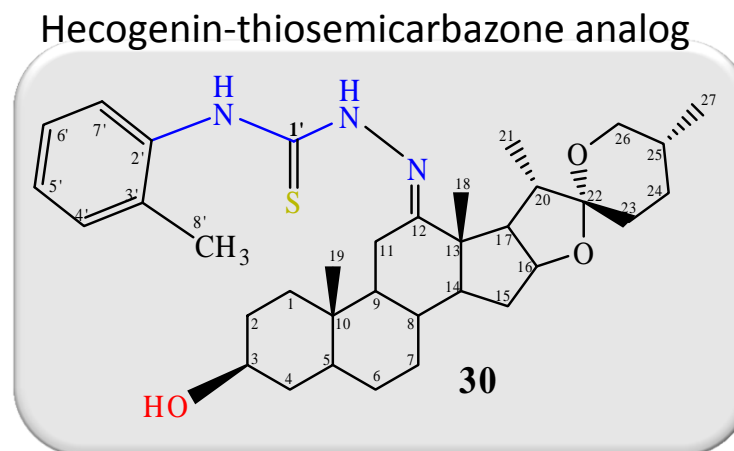
17. Wu, C.; Shukla, S.; Calcagno, A.M.; Hall, M. D.; Gottesman, M.M.; Ambudkar, S.V. *Mol. Cancer Ther.* **2007**, *6*, 3287-3296.
18. Breast cancer: prevention and control.
<http://www.WHO.int/cancer/detection/breastcancer/en/> **2016**. Accessed May 25, 2016.
19. Global burden of disease cancer collaboration, The global burden of cancer 2013, *JAMA Oncol.* **2015**, *1*, 505-527.
20. Hoelder, S.; Clarke, P.A.; Workman, P. *Oncol.* **2012**, *6*, 155-176.
21. Walsh, C. T. Posttranslational modification of proteins: Expanding nature's inventory, Englewood, Colo.: Roberts and Co. Publishers. XXI, **2006**, 490.
22. Ren, R. *Nat. Rev. Cancer.* **2005**, *5*, 172-183.
23. Pearson, G.; English, J.M.; White, M.A.; Cobb, M.H. *J. Biol. Chem.* **2001**, *276*, 7927-7931.
24. Pages, G.; Lenormand, P.; L'Allemain, G.; Chambard, J.C.; Meloche, S.; Pouyssegur, J. *Proc. Natl. Acad. Sci. U.S.A.* **1993**, *90*, 8319-8323.
25. Sears, R.C.; Nevins, J.R. *J. Biol. Chem.* **2002**, *277*, 11617-11620.
26. English, J. M.; Cobb, M.H. *Trends Pharmacol. Sci.* **2002**, *23*, 40-45.
27. Robbins, D.J.; Zhen, E.; Owaki, H.; Vanderbilt, C.A.; Ebert, D.; Geppert, T.D.; Cobb, M.H. *J. Biol. Chem.* **1993**, *268*, 5097-5105.
28. Adjei, A.A.; Cohen, R.B.; Franklin, W.; Morris, C.; Wilson, D.; Molina, J.R.; Hanson, L.I.; Gore, L.; Chow, L.; Leong, S. *J. Clin. Oncol.* **2008**, *26*, 2139-2146.

29. Ascierto, P.A.; Schadendorf, D.; Berking, C.; Agarwala, S.S.; van Herpen, C.M.; Queirolo, P.; Blank, C.U.; Hauschild, A.; Beck, J. T.; St-Pierre, A. *Lancet Oncol.* **2013**, *14*, 249-256.
30. Trametinib and Dabrafenib. <http://www.fda.gov/drugs/informationondrugs/approveddrugs>. Accessed June 9, 2016.
31. Holliday, D.L.; Speirs, V. *Breast Cancer Res.* **2011**, *13*, 215-221.
32. Glide, version 5.8, Schrödinger, LLC; New York, NY, USA, **2012**.
33. Roskoski Jr., R. *Biochem. Biophys. Res. Comm.* **2012**, *417*, 5-10.
34. Leung, E.Y.; Kim, J.E.; Askarian-Amiri, M.; Rewcastle, G.W.; Finlay, G.J.; Baguley, B.C. *PLoS One* **2014**, *9*, e105792.
35. Smith, M. B. Organic chemistry, an acid-base approach. CRC Press, Taylor and Francis Group, **2011**, 872.
36. Serda, M.; Kalinowski, D.S.; Rasko, N.; Potůčková, E.; Mrozek-Wilczkiewicz, A.; Musiol, R.; Małecki, J.G.; Sajewicz, M.; Ratuszna, A.; Muchowicz, A.; Gołąb, J.; Simůnek, T.; Richardson, D.R.; Polanski, J. *PLoS One* **2014**, *9*, e110291.
37. Soule, H.D.; Maloney, T.M.; Wolman, S.R.; Peterson, W.D.; Brenz, R.; McGrath, C.M.; Russo, J.; Pauley, R.J.; Jones, R.F.; Brooks, S.C. *Cancer Res.* **1990**, *50*, 6075–6086.
38. Huang, R.; Southall, N.; Cho, M.; Xia, M.; Inglese, J.; Austin, C.P. *Chem. Res. Toxicol.* **2008**, *21*, 659-667.
39. Clark, A. G.; Vignjevic, D. M. *Curr. Opin. Cell Biol.* **2015**, *36*, 13-22.
40. Arthur, J.S. *Front. Biosci.* **2008**, *13*, 5866-5879.

41. M. Buxade, J.L. Parra-Palau, C.G. Proud. *Front. Biosci.* **2008**, *13*, 5359-5373.
42. RCSB Protein Data Bank. <http://www.rcsb.org/pdb/home/home.do>. Accessed April 10, 2016.
43. Friesner, R.A.; Murphy, R.B.; Repasky, M.P.; Frye, L.L.; Greenwood, J.R.; Halgren, T.A.; Sanschagrin, P.C.; Mainz, D.T. *J. Med. Chem.* **2006**, *49*, 6177-6196.
44. Elsayed, H.E.; Akl, M.R.; Ebrahim, H.Y.; Sallam, A.A.; Haggag, E. G.; Kamal, A.M.; El Sayed, K.A. *Chem. Biol. Drug Des.* **2015**, *85*, 231–243.
45. Cultrex[®] BME cell invasion assay protocol. www.trevigen.com. Accessed June 9, 2016.
46. Ebrahim, H.Y.; Elsayed, H.E.; Mohyeldin, M.M.; Akl, M.R.; Bhattacharjee, J.; Egbert, S.; El Sayed, K.A. *Phytother. Res.* **2016**, *30*, 557-566.
47. Akl, M.R.; Elsayed, H.E.; Ebrahim, H.Y.; Haggag, E.G.; Kamal, A.M.; El Sayed, K.A. *Eur. J. Pharmacol.* **2014**, *740*, 209–217.



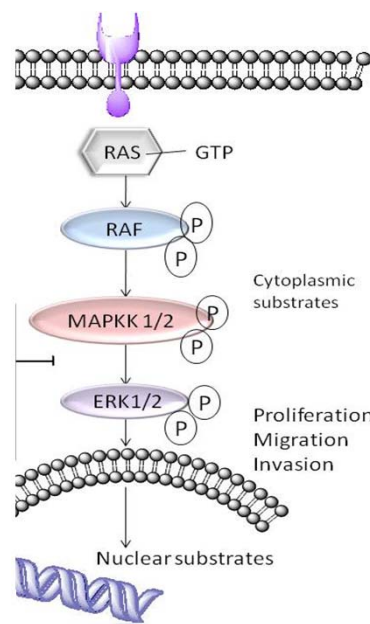
In vitro IC₅₀ = 28.7 μM



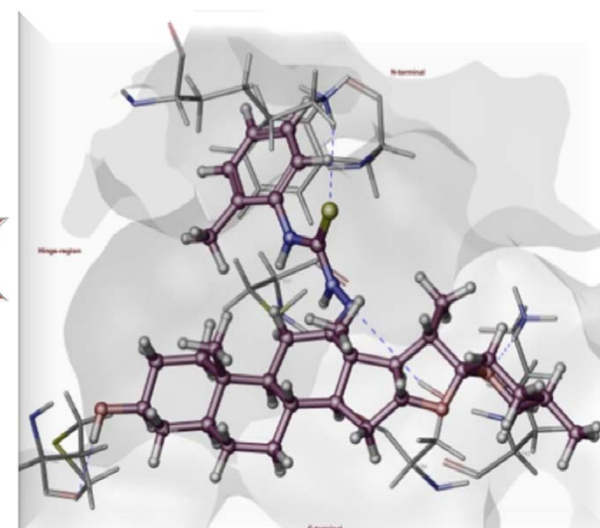
In vitro IC₅₀ = 1.9 μM



In vivo efficacy model



Molecular Target



Molecular Docking